

AEDC-TDR-62-230

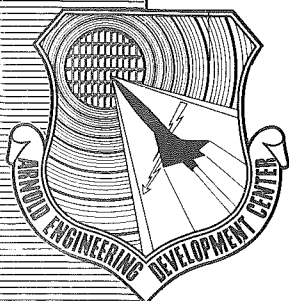
10 MAY 1963

MAY 15 1963

JUL 10 1963

AUG 28 1963

APR 19 1964



# AERODYNAMIC DESIGN AND CALIBRATION OF THE VKF 50-INCH HYPERSONIC WIND TUNNELS

By

James C. Sivells

von Kármán Gas Dynamics Facility  
ARO, Inc.

TECHNICAL DOCUMENTARY REPORT NO. AEDC-TDR-62-230

March 1963

PROPERTY OF U. S. AIR FORCE  
AEDC LIBRARY  
AF 40(600)1000

AFSC Program Area 040A

(Prepared under Contract No. AF 40(600)-1000 by ARO, Inc.,  
contract operator of AEDC, Arnold Air Force Station, Tenn.)

**ARNOLD ENGINEERING DEVELOPMENT CENTER**  
**AIR FORCE SYSTEMS COMMAND**  
**UNITED STATES AIR FORCE**

# *NOTICES*

Qualified requesters may obtain copies of this report from ASTIA. Orders will be expedited if placed through the librarian or other staff member designated to request and receive documents from ASTIA.

When Government drawings, specifications or other data are used for any purpose other than in connection with a definitely related Government procurement operation, the United States Government thereby incurs no responsibility nor any obligation whatsoever; and the fact that the Government may have formulated, furnished, or in any way supplied the said drawings, specifications, or other data, is not to be regarded by implication or otherwise as in any manner licensing the holder or any other person or corporation, or conveying any rights or permission to manufacture, use, or sell any patented invention that may in any way be related thereto.

AERODYNAMIC DESIGN AND CALIBRATION  
OF THE  
VKF 50-INCH HYPERSONIC WIND TUNNELS

By  
James C. Sivells  
von Kármán Gas Dynamics Facility  
ARO, Inc.  
a subsidiary of Sverdrup and Parcel, Inc.

March 1963

ARO Project Nos. 345801  
340925  
357802  
355956

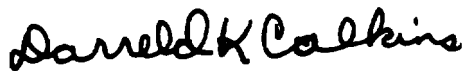


**ABSTRACT**

The theoretical and empirical methods used in the aerodynamic design of the 50-Inch Mach 8 Tunnel (B) and the 50-Inch Mach 10 Tunnel (C) are described. Both tunnels have axisymmetric contoured nozzles. Calibration data concerning Mach number distribution, boundary-layer thickness, and diffuser performance are also presented.

**PUBLICATION REVIEW**

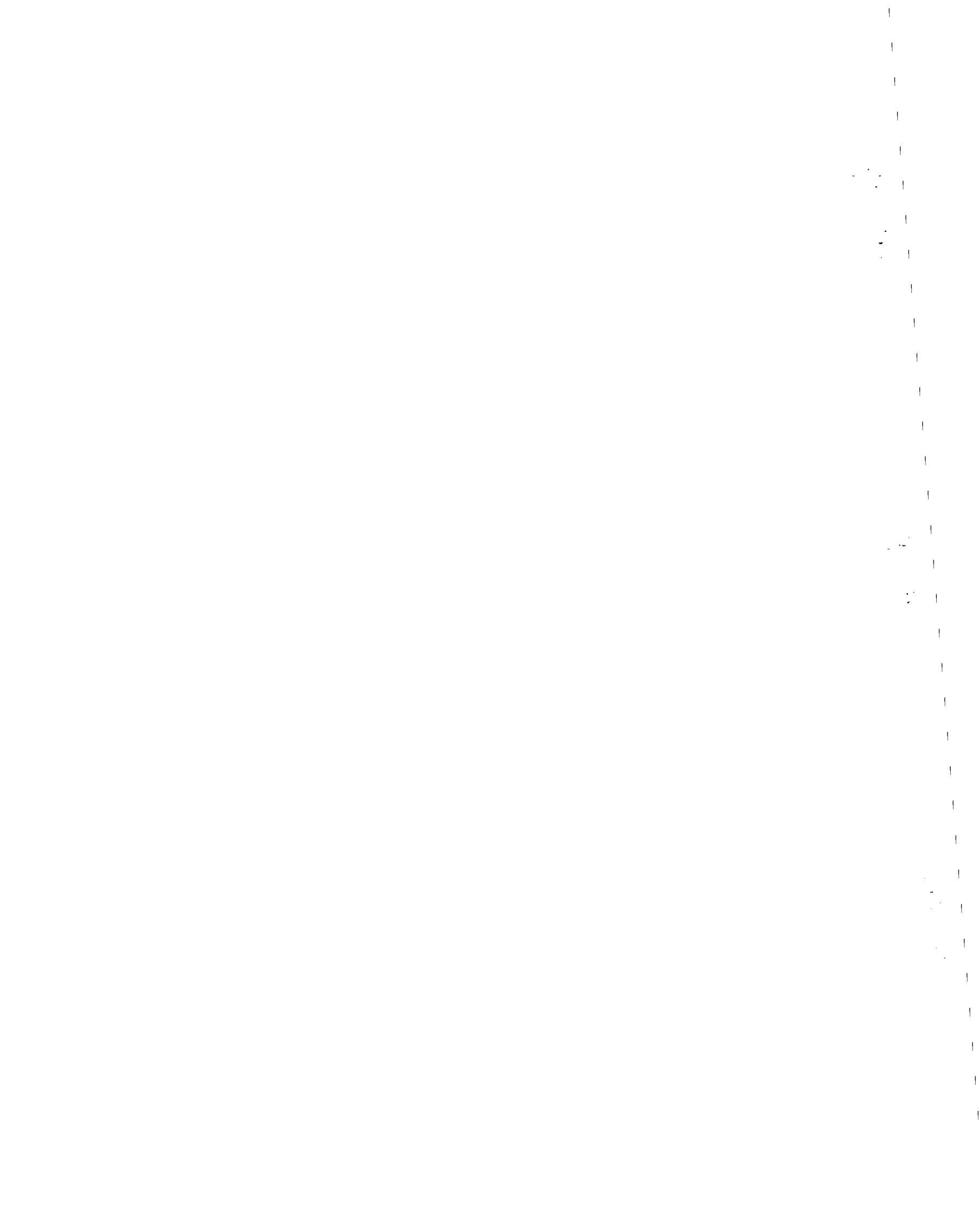
This report has been reviewed and publication is approved.



Darreld K. Calkins  
Major, USAF  
AF Representative, VKF  
DCS/Test



Jean A. Jack  
Colonel, USAF  
DCS/Test



## CONTENTS

	<u>Page</u>
ABSTRACT. . . . .	iii
NOMENCLATURE. . . . .	vii
1.0 INTRODUCTION . . . . .	1
2.0 NOZZLE DESIGN	
2.1 Downstream Contour . . . . .	2
2.2 Supersonic Contour . . . . .	6
2.3 Subsonic Contour . . . . .	7
2.4 Boundary-Layer Correction . . . . .	7
2.5 Application. . . . .	9
3.0 FABRICATION . . . . .	13
4.0 CALIBRATION	
4.1 Stagnation Temperature Distribution . . . . .	14
4.2 Mach Number Distribution. . . . .	14
4.3 Flow Angularity Survey . . . . .	17
4.4 Boundary-Layer Survey . . . . .	18
4.5 Diffuser Performance. . . . .	18
5.0 CONCLUDING REMARKS . . . . .	20
REFERENCES . . . . .	20

## TABLES

1. Pertinent Dimensions of Axisymmetric Nozzles . . . . .	23
2. Coordinates of Mach 8 Contour . . . . .	24
3. Coordinates of Mach 10 Contour . . . . .	25
4. Coordinates of Mach 12 Contour . . . . .	26

## ILLUSTRATIONS

Figure

1. The 50-Inch Mach 8 Tunnel (B)	
a. General Arrangement . . . . .	27
b. View Looking Downstream . . . . .	28
2. The 50-Inch Mach 10 Tunnel (C)	
a. General Arrangement . . . . .	29
b. View Looking Downstream . . . . .	30

<u>Figure</u>	<u>Page</u>
3. Downstream Inviscid Contour. . . . .	31
4. Throat Contour . . . . .	32
5. Comparison of Theoretical and Empirical Inviscid Contours	
a. Mach 10 . . . . .	33
b. Mach 12 . . . . .	33
6. Comparison of Theoretical and Empirical Mach Number Distribution. . . . .	34
7. Inviscid Contours for the Mach 10 and 12 Nozzles Compared to the Physical Contour for Mach 10. . . . .	35
8. Air Temperatures Measured in the Mach 8 Tun- nel (B) Instrumentation Ring as Viewed Looking Downstream; Stagnation Pressure = 500 psia; Inside Diameter of Instrumentation Ring = 26 in. ; Temperatures in °F . . . . .	36
9. Air Temperatures Measured in the Mach 10 Tun- nel (C) Instrumentation Ring as Viewed Looking Downstream; Stagnation Pressure = 1600 psia; Inside Diameter of Instrumentation Ring = 12 in. ; Temperatures in °F . . . . .	37
10. Mach Number Distribution in the Mach 8 Tunnel (B). . . . .	38
11. Centerline Mach Number Variation with and without Known Disturbances . . . . .	39
12. Pressure Distributions Measured on a Hemispherical Nose of a Model Located at Two Positions in the Mach 8 Tunnel (B) . . . . .	40
13. Mach Number Distribution in the Mach 10 Tunnel (C) . . . . .	41
14. Shadowgram of Flow Angularity Probe. . . . .	42

## NOMENCLATURE

A	Area
$C_0, C_1, C_2, C_3$	Constants, Eqs. (9) through (14)
$C_f$	Skin friction coefficient
c, d	Constants, Eq. (28)
F, f, G, g	Constants, Eq. (29)
H	Boundary-layer form factor
$H_{tr}$	Transformed form factor
M	Mach number
$p_0$	Stagnation pressure
R	Radius of curvature
r	Radial distance from source
$r_1$	Radial distance from source to where $M = 1$
$T_w$	Wall temperature
V	Velocity
W	Dimensionless velocity
X	Distance along axis of nozzle from throat
x	Distance along axis from theoretical source
Y	Physical ordinate, including boundary-layer correction, measured normal to axis
y	Distance normal to axis
$\alpha$	Stream angle
$\beta$	Azimuth angle on hemisphere
$\gamma$	Ratio of specific heats
$\delta^*$	Boundary-layer displacement thickness
$\theta$	Angle of subsonic contour
$\phi$	Angle of inviscid contour
$\psi$	Prandtl-Meyer angle in two-dimensional flow
$\psi'$	Expansion angle in radial flow

$\omega$  Angle at inflection point of inviscid contour  
 $\omega'$  Angle at inflection point of contour with  
boundary-layer correction

**SUBSCRIPTS**

A, A', a, B, b, C, D, E Value at points located in Figs. 3 and 4  
RG Evaluated for a real gas

**SUPERSCRIPT**

\* Evaluated at  $M = 1$  except  $\delta^*$

## 1.0 INTRODUCTION

Among the various wind tunnels of the von Kármán Gas Dynamics Facility (VKF) of the Arnold Engineering Development Center (AEDC), Air Force Systems Command (AFSC), are two 50-in. -diam hypersonic wind tunnels, the Mach 8 Tunnel (B) and the Mach 10 Tunnel (C). Both tunnels are continuously operated with air supplied by the VKF 92, 500-hp main compressor system. For the Mach 8 Tunnel (B), seven compressor stages supply air at stagnation pressures from 100 to 900 psia with stagnation temperatures up to 900°F obtained through the use of a propane-fired combustion heater. For the Mach 10 Tunnel (C), eight compressor stages supply air at stagnation pressures from 200 to 2000 psia with stagnation temperatures up to 1450°F obtained with a combination of the combustion heater and a 12,000-kw electrical resistance heater. These temperatures are sufficient to prevent liquefaction of the air when it is expanded to test section conditions.

In order to provide the best quality of aerodynamic data from model tests, it is desirable for the airflow in the test region to have uniform velocity with no tunnel-induced disturbances. The extent to which this goal is achieved depends upon the design and fabrication of the wind tunnel. The purpose of this report is to describe the methods used to design the VKF hypersonic tunnels and to present the results of their calibrations.

Although good results at supersonic speeds have been obtained with two-dimensional nozzles, there is an upper limit in Mach number for which such nozzles are practical. As the Mach number increases, the area ratio increases rapidly so that the resulting throat height decreases to such a small dimension that normal machining tolerances become appreciable percentages of that dimension. Also, as the Mach number increases, the stagnation temperature required to prevent liquefaction increases and the amount of cooling required to maintain dimensional stability increases. The maximum heat-transfer rate occurs in the vicinity of the throat, and any nonuniformity in cooling results in uneven expansions which are also appreciable percentages of the throat dimension. Such problems are shown in Ref. 1 to be alleviated to some extent by using axisymmetric nozzles. An additional advantage of an axisymmetric nozzle is that there is no transverse pressure gradient, such as that found on the sidewalls of a two-dimensional nozzle. Such transverse gradients produce transverse variations in boundary-layer thickness (Ref. 1) which cannot be taken into account in the design of the nozzle.

---

Manuscript received February 1963.

For the above reasons, the VKF 50-in. -diam hypersonic tunnels have axisymmetric nozzles. These tunnels are the largest of their type known to be in operation. Chronologically, the Mach 8 Tunnel was constructed first and has been operational since October 1958. Its general arrangement is shown in Fig. 1, and details of its operation are given in Ref. 2. The Mach 10 Tunnel (C) has been operational since May 1960, and its general arrangement is shown in Fig. 2. The design of many of its unique details is given in Ref. 3, and the stress and thermal analysis of its throat section are given in Ref. 4.

## 2.0 NOZZLE DESIGN

The aerodynamic design of an axisymmetric nozzle can be divided into two parts; namely, the inviscid or potential-flow contour, and the correction required to account for the longitudinal growth of the boundary layer. The inviscid contour can be further divided into three parts; the downstream contour from the inflection point to the test section, the supersonic contour from the throat to the inflection point, and the subsonic contour upstream of the throat. Each part of the design will be described separately.

### 2.1 DOWNSTREAM CONTOUR

#### 2.1.1 Description

The downstream inviscid contours were designed by the method of Ref. 5. As illustrated in Fig. 3, the assumption is made that the flow originates from a spherical source at point 0 and flows radially until the axisymmetric characteristic AB is reached. The nozzle is therefore conical to the inflection point A with a cone half-angle  $\omega$ . Downstream of the characteristic CD, where the test model is to be located, the flow is uniform and parallel to the nozzle axis. In the region ABCD, the transition is made from radial flow to parallel flow. Flow velocity and direction in this region must be determined by the method of axisymmetric characteristics. What must be determined, then, is the streamline AD which is the inviscid contour downstream of the inflection point.

The shortest possible nozzle for a given cone angle would be obtained if the points B and C coincided. In such a nozzle, however, the Mach number gradient along the axis would be discontinuous at the point B and the curvature of the nozzle would be discontinuous at the inflection point. Theoretically, a discontinuity in curvature could be

machined into the nozzle if the boundary-layer correction could be neglected. The boundary-layer growth is smoother, however, if the curvature is continuous. Moreover, even if the boundary-layer growth could be calculated exactly, only the correction at design operating conditions can be applied to the contour. Therefore, deviations in boundary-layer growth at off-design operating conditions would cause the discontinuity to occur at the wrong location along the nozzle with the result that there would be disturbances in the flow in the test region. These conditions are alleviated if the contour has continuous curvature.

Continuous curvature is obtained in the method of Ref. 4 by using a region of partial cancellation which is represented along the nozzle axis by the length  $x_{BC}$ . The Mach number at the point B,  $M_B$ , is arbitrarily fixed, and the distribution of the velocity parameter  $W$  is described as a function of  $x$  by a cubic equation in which the Mach number gradient is continuous at the point B and is zero at the point C. The second derivative of  $M$  with respect to  $x$  is also zero at the point C. The constants in the cubic equation and the length  $x_{BC}$  are then found to match these conditions.

A slightly more complicated procedure of describing the Mach number distribution along  $x_{BC}$  is given in Ref. 6. In addition in the preceding conditions, the second derivative of  $M$  with respect to  $x$  is made continuous at the point B and the length  $x_{BC}$  is fixed. These additional conditions require that a fifth-degree polynomial be used to express  $M$  as a function of  $x$ . It is not known if contours obtained by this method produce any more uniform flow than those obtained by the method of Ref. 5.

### 2.1.2 Analysis

In the radial flow region, the radial distance from the source to the spherical segment where the velocity is sonic is designated as  $r_1$ . All dimensions in Ref. 5 are made nondimensional by making  $r_1$  equal to unity. The sonic area is the area of the spherical segment

$$A^* = 2\pi r_1^2 (1 - \cos \omega) \quad (1)$$

At any succeeding spherical segment, the Mach number is given by the relation

$$\frac{1}{M} \left( \frac{\gamma-1}{\gamma+1} M^2 + \frac{2}{\gamma+1} \right)^{\frac{\gamma+1}{2(\gamma-1)}} = \frac{A}{A^*} = \frac{r^2}{r_1^2} \quad (2)$$

At the inflection point,

$$\frac{r_A}{r_1} = M_A^{-1/2} \left( \frac{\gamma-1}{\gamma+1} M_A^2 + \frac{2}{\gamma+1} \right)^{\frac{\gamma+1}{4(\gamma-1)}} \quad (3)$$

and at the point B,

$$\frac{r_B}{r_1} = M_B^{-1/2} \left( \frac{\gamma-1}{\gamma+1} M_B^2 + \frac{2}{\gamma+1} \right)^{\frac{\gamma+1}{4(\gamma-1)}} \quad (4)$$

As shown in Ref. 7, the expansion angle  $\psi'$  in radial flow is one-half the Prandtl-Meyer expansion angle  $\psi$  in two-dimensional flow:

$$2\psi' = \psi = \sqrt{\frac{\gamma+1}{\gamma-1}} \tan^{-1} \sqrt{\frac{\gamma-1}{\gamma+1} (M^2 - 1)} - \tan^{-1} \sqrt{M^2 - 1} \quad (5)$$

Therefore, the Mach numbers at points A and B are also related by

$$\psi_B - \psi_A = 2\omega \quad (6)$$

Of course, all intermediate points along the right running or second family characteristic AB are also defined through the use of the same general relationships.

In Ref. 5, all velocities are made nondimensional by dividing by the velocity at the throat to give the velocity ratio W which is related to the Mach number by

$$W^2 = \left( \frac{V}{V^*} \right)^2 = \frac{\frac{\gamma+1}{\gamma-1} M^2}{M^2 + \frac{2}{\gamma-1}} \quad (7)$$

At the end of the radial flow region, by differentiating Eqs. (2) and (7),

$$\left( \frac{dW}{dx} \right)_B = \frac{2 W_B \left( \frac{\gamma+1}{\gamma-1} - W_B^2 \right)}{\frac{\gamma+1}{\gamma-1} r_B (W_B^2 - 1)} \quad (8)$$

The velocity ratio from points B to C on the axis is arbitrarily defined by the equation

$$W = C_0 + C_1 \frac{x - x_B}{x_{BC}} + C_2 \left( \frac{x - x_B}{x_{BC}} \right)^2 + C_3 \left( \frac{x - x_B}{x_{BC}} \right)^3 \quad (9)$$

The constants in Eq. (8) are evaluated by the end conditions at  $x_B$ ,

$$W = W_B$$

$$\frac{dW}{dx} = \left(\frac{dW}{dx}\right)_B$$

and at  $x_C$ ,

$$W = W_C$$

$$\frac{dW}{dx} = 0$$

$$\frac{d^2W}{dx^2} = 0$$

to give

$$C_0 = W_B \quad (10)$$

$$C_1 = 3(W_C - W_B) \quad (11)$$

$$C_2 = -3(W_C - W_B) \quad (12)$$

$$C_3 = W_C - W_B \quad (13)$$

$$x_{BC} = \frac{C_1}{\left(\frac{dW}{dx}\right)_B} = \frac{3(W_C - W_B) \frac{\gamma + 1}{\gamma - 1} r_B (W_B^2 - 1)}{2 W_B \left(\frac{\gamma + 1}{\gamma - 1} - W_B^2\right)} \quad (14)$$

Thus, all the conditions of velocity, flow direction, and Mach angle can be determined at as many points as desired along characteristic AB and line BC for the purpose of calculating a characteristic network in the transition region. The characteristic solution must be obtained by a numerical step-by-step procedure using finite differences since no analytic solution is available. The assumptions made in Ref. 7 are not sufficiently accurate for this purpose even for a minimum-length nozzle.

The transition region is terminated by the left running or first family characteristic CD which is straight since  $M_C = M_D$ . The coordinates of point D can be calculated since

$$\frac{\pi y_D^2}{2 \pi r_1^2 (1 - \cos \omega)} = \frac{A_D}{A^*} \quad (15)$$

or

$$\frac{y_D}{r_1} = 2 \sqrt{\frac{A_D}{A^*}} \sin \frac{\omega}{2} \quad (16)$$

and

$$\frac{x_{CD}}{r_1} = 2 \sqrt{(M_{CD}^2 - 1)} \frac{A_D}{A^*} \sin \frac{\omega}{2} \quad (17)$$

since the angle between CD and the axis is the Mach angle.

The length of the downstream contour is

$$x_D - x_A = r_B - r_A \cos \omega + x_{BC} + x_{CD} \quad (18)$$

where the parameters for a nondimensional nozzle for a given Mach number  $M_{CD}$  are the cone angle  $\omega$  and the Mach number  $M_B$ . The contours of Ref. 5 all have a constant value of  $M_{CD} - M_B = 0.2$ . The nondimensional coordinates must, of course, be multiplied by a scale factor equal to  $r_1$  to match the linear dimensions of the nozzle.

## 2.2 SUPERSONIC CONTOUR

The throat contour is illustrated in Fig. 4. The selection of the supersonic contour was arbitrary since no theoretical contour was available to produce the desired radial flow. It was believed that the contour should monotonically increase to the point of tangency with the cone angle  $\omega'$  where the curvature should be zero. The cone angle  $\omega'$  is the cone angle  $\omega$  after the boundary-layer correction is added. The corrected cone angle was selected because the supersonic contour was arbitrary in the first place, and secondly, the boundary-layer calculation in this region would be influenced by real gas effects and would require more approximations than that further downstream where the flow expands to such low pressure and temperature that it more nearly approximates a perfect gas.

On a one-dimensional basis, it was found that a semi-cubic equation produced what appeared to be a desirable Mach number distribution. The resulting equation was

$$\left(\frac{Y}{Y^*}\right)^2 = 1 + \left[\frac{Y^*}{R^*} \left(\frac{X_b}{Y^*}\right)^2\right] \left[\left(\frac{X}{X_b}\right)^2 - \frac{1}{3} \left(1 - \frac{R^*}{Y^*} \tan^2 \omega'\right) \left(\frac{X}{X_b}\right)^3\right] \quad (19)$$

where the coordinates at the point of tangency (Fig. 4) are

$$\frac{X_b}{Y^*} = 2 \frac{R^*}{Y^*} \tan \omega' \left[ \frac{3}{\left(3 + \frac{R^*}{Y^*} \tan^2 \omega'\right) \left(1 - \frac{R^*}{Y^*} \tan^2 \omega'\right)} \right]^{1/2} \quad (20)$$

and

$$\frac{Y_b}{Y^*} = \left(1 + \frac{R^*}{Y^*} \tan^2 \omega'\right) \left[ \frac{3}{\left(3 + \frac{R^*}{Y^*} \tan^2 \omega'\right) \left(1 - \frac{R^*}{Y^*} \tan^2 \omega'\right)} \right]^{1/2} \quad (21)$$

The throat radius  $Y^*$  was calculated from the area ratio and the value of  $y_D$  from Eq. (16):

$$Y^* = \frac{y_D}{\left(\frac{A_D}{A^*}\right)_{RG}^{1/2}} \quad (22)$$

where in this case real gas effects must be taken into account even though they were neglected in Eq. (1) and the subsequent derivation of the downstream contour.

### 2.3 SUBSONIC CONTOUR

The selection of the subsonic contour was even slightly more arbitrary than that of the supersonic contour. A cubic equation was selected which had the same radius of curvature at the throat as the supersonic contour,

$$\frac{Y}{Y^*} = 1 + 2 \frac{R^*}{Y^*} \tan^2 \theta \left(\frac{X}{X_a}\right)^2 - \frac{2}{3} \frac{R^*}{Y^*} \tan^2 \theta \left(\frac{X}{X_a}\right)^3 \quad (23)$$

where the coordinates at the point a (Fig. 4) are

$$\frac{X_a}{Y^*} = 2 \frac{R^*}{Y^*} \tan \theta \quad (24)$$

and

$$\frac{Y_a}{Y^*} = 1 + \frac{4}{3} \frac{R^*}{Y^*} \tan^2 \theta \quad (25)$$

Also at the point a, the slope of the cubic is  $\tan \theta$  and the second derivative is zero. Thus another arbitrary variable,  $\tan \theta$ , is introduced to allow the tangent line to pass through any selected point E, such as the end of the stilling chamber.

### 2.4 BOUNDARY-LAYER CORRECTION

To each value of  $y$  along the contour AD must be added the boundary-layer correction,  $\delta^* \sec \phi$ , to obtain the value of  $Y$  to define the physical contour of the nozzle. For the range of operating conditions of the VKF 50-in. hypersonic tunnels, the boundary layer is turbulent for the full length of the nozzle. Because of the meager amount of experimental data on boundary-layer growth at hypersonic speeds, many empirical methods have been developed which attempt to apply low-speed data to flow at supersonic and hypersonic speeds. For the Mach 8 Tunnel (B), the method used to calculate the boundary-layer growth was one in which the reference temperature was the arithmetic mean between free-stream and wall temperature. During the fabrication and early operation of the tunnel, an improved method was developed which correlated very well with experimental measurements made in an earlier conical nozzle and in the

contoured nozzle. In this improved method, described in Ref. 8, a modification of Stewartson's transformation was used to simplify the integration of the von Kármán momentum equation. Heat transfer between the air and the tunnel wall was taken into account approximately by evaluating the air properties at Eckert's reference temperature and by using the adiabatic-wall temperature instead of the stagnation temperature in Crocco's quadratic for the temperature distribution in the boundary layer. The final equation for the boundary-layer displacement thickness is, assuming zero thickness at the throat,

$$\delta^* = \frac{\left(1 + \frac{\gamma-1}{2} M^2\right)^{\frac{\gamma+1}{2(\gamma-1)}} H}{y M^{2+H_{tr}}} \int_0^X \frac{y M^{2+H_{tr}} C_{f/2}}{\left(1 + \frac{\gamma-1}{2} M^2\right)^{\frac{\gamma+1}{2(\gamma-1)}}} \sec \phi dX \quad (26)$$

Because of the excellent correlation obtained at Mach 8, Eq. (26) was used to calculate the growth of the boundary-layer displacement thickness for the Mach 10 Tunnel (C) and for the Mach 12 nozzle from which the Mach 10 nozzle parameters were derived.

Inasmuch as the aerodynamic design of the nozzle must precede the detailed calculations of the heat exchanged from the nozzle air to the water used to cool the nozzle, an approximation must be made of the nozzle wall temperature for use in the boundary-layer calculations. It was assumed that the wall temperature along the contour AD was constant at 530°R, the cooling water temperature, and from the throat to the inflection point A,

$$T_w = 530^\circ\text{R} + \left(\frac{T_w^* - 530^\circ\text{R}}{A_A/A^* - 1}\right) \left(\frac{A_A/A^*}{A/A^*} - 1\right) \quad (27)$$

The assumed values of  $T_w^*$  at the throat were 960°R for Mach 8, 1000°R for Mach 10, and 1200°R for Mach 12. The final values obtained by a heat balance in Ref. 4 were 1059°R for Mach 10 and 1114°R for Mach 12 for maximum operating conditions. Fortunately, the choice of the wall temperature does not seriously influence the boundary-layer calculations.

A further approximation was needed to compute the boundary-layer growth according to Eq. (26). The Mach number variation along the contour AD was not given with the contour in Ref. 5. The following approximation was developed:

$$(M - c)^2 = (M_D - c)^2 + d (x - x_D)^3 \quad (28)$$

where

$$d = \frac{2(M_A - c) (dM/dx)_A}{3(x_D - x_A)^2}$$

$$c = \frac{M_D^2 - M_A^2 - 2/3 (dM/dx)_A (x_D - x_A) M_A}{2M_D - 2M_A - 2/3 (dM/dx)_A (x_D - x_A)}$$

$$\left(\frac{dM}{dx}\right)_A = \frac{(\gamma - 1) M_A \left(M_A^2 + \frac{2}{\gamma - 1}\right)}{x_A (M_A^2 - 1)}$$

Equation (28) satisfies the conditions that  $M = M_A$  and  $dM/dx = (dM/dx)_A$  when  $x = x_A$ , and  $M = M_D$ ,  $dM/dx = 0$ , and  $(d^2M)/(dx^2) = 0$  when  $x = x_D$ .

It is realized that the procedure of correcting the inviscid contour by adding to it the boundary-layer displacement thickness is at best only an approximation. The characteristic curves are not reflected from the streamline surface at the edge of the displacement thickness in the same manner in which they theoretically reflect from a solid surface in inviscid flow. The approximation is reasonable, moreover, only when the displacement thickness is relatively small as compared with the radius of the inviscid contour. When the displacement thickness becomes an appreciable part of the total radius, it appears that a better approximation may be the method of Ref. 9 adapted for turbulent flow. This method, however, requires considerable iteration to obtain the desired physical contour since it determines the growth of an internal boundary layer.

## 2.5 APPLICATION

### 2.5.1 Mach 8 Tunnel (B)

At the time the Mach 8 nozzle was being designed, there was in operation in the same location a 50-in. -diam conical nozzle with interchangeable throats for Mach 7 and 8. The conical nozzle was primarily intended for the shakedown of the compressor plant and combustion heater. A few aerodynamic tests were attempted, however, in spite of the Mach number gradient inherent in a conical nozzle and flow irregularities attributable to the method of fabrication. This nozzle dictated most of the design dimensions of the Mach 8 contoured nozzle; the diameter at the upstream end of the subsonic contour was 12 in., the throat section was 25 in. long to a point where the maximum nozzle diameter was 5 in., the center of model rotation in the test section was 278 in., and the end of the test section was 50 in. in diameter and 298 in. from the beginning of the subsonic contour. In addition to these criteria, it was decided that the terminal characteristic CD should clear the nose of a model (45 in. long from its nose to the center of rotation) at an angle of attack of 15 deg, and that the

curved part of the contour should end 40 in. upstream of the end of the test section where it would be approximately tangent to a 40-in. -long conical section. The design operating conditions were a stagnation pressure of 600 psia and a stagnation temperature of 1360°R.

Using these criteria, a cone half-angle was selected from those for which contours were available in Ref. 5. By means of an iteration process, a scale factor  $r_1$  was selected for multiplying the coordinates of the downstream contour, a boundary layer was estimated, the subsonic and supersonic contours were calculated, and the complete contour was plotted to determine how well it satisfied the criteria. This process was repeated until the desired conditions were satisfied. Because of the restriction of a 5-in. diameter at a station 25 in. downstream of upstream end of the subsonic contour and because it was believed that it would be easier to machine conical contours at this station, the maximum ratio of throat-radius-of-curvature to throat radius was 5, although a larger value was believed to be desirable. The only available value of cone half-angle that would satisfy the criteria was 12 deg. Values of the final pertinent dimensions are given in Table 1 and the coordinates in Table 2.

### 2.5.2 Mach 10 Tunnel (C)

The Mach 10 nozzle was designed so that it would be replaced later with a Mach 12 nozzle. Moreover, it was thought that the same downstream contour, corrected for the boundary-layer displacement thickness, might be usable for both Mach numbers. If this idea proved to be practical, only the sections upstream of the inflection point would need to be interchanged. Since these sections are relatively short, a considerable saving would be effected, not only in initial cost, but also in the time required each time the sections are changed. In order to match the downstream section, both upstream sections must have the same ordinate and slope at the inflection point after the boundary-layer correction is made. If it is found later in the calibration that separate downstream sections are required, at least nothing will have been lost by adopting this philosophy.

Inasmuch as the nozzle length increases with Mach number for the same value of  $\omega$  and  $M_{CD} - M_B$ , it was necessary to first determine the Mach 12 contour and then adjust the value of  $M_{CD} - M_B$  to produce a Mach 10 contour of the same length. It was believed that the downstream contours would be more nearly alike if the cone half-angle was small since the nozzle length would be enough to produce a relatively large boundary layer which would tend to mask differences in the contours. It is desirable, on the other hand, to keep the nozzle length short

enough that the boundary layer does not make the test core too small. From these desiderations, a cone half-angle of 8 deg was selected for the Mach 12 nozzle.

Other design criteria were: at station 0 upstream of the subsonic contour the diameter to be 12 in., the ratio of throat-radius-of-curvature to throat radius to be 35, the inflection point to be at station 54, at station 316 the diameter to be 48.5 in., at station 370 the diameter to be 50 in., the contour to be conical from station 316 to station 370, the model center of rotation to be at station 350, and the characteristic CD to clear the nose of a model (45 in. long from its nose to the center of rotation) at an angle of attack of 15 deg. The last criterion could have been relaxed since the maximum model length which can be injected into the tunnel is 30 in. from its nose to the nominal center of rotation (Ref. 3). However, this criterion might have been replaced by one calling for a shorter model at a higher angle of attack. The design operating conditions were a stagnation pressure of 1500 psia and an ideal gas stagnation temperature of 2520°R. The ideal gas value was used so that standard tables for  $\gamma = 1.4$  could be used to determine the static temperature for the boundary-layer calculations.

Some of the design criteria were interdependent and were established in the course of finding a scale factor for the nondimensional coordinates for the downstream contour. The procedure of determining the scale factor was iterative as for the Mach 8 nozzle, but, with the background of the previous nozzle, the boundary-layer correction was obtained by the method of Ref. 8. The final pertinent dimensions are listed in Table 1.

The design criteria for the Mach 10 nozzle were the same as for the Mach 12 nozzle except that the ratio of throat-radius-of-curvature to throat radius was 30 and the design, ideal gas stagnation temperature was 1985°R. Two additional criteria were added: the ordinate and the slope at the inflection point after boundary-layer correction must be the same for both nozzles. These added criteria made the problem more difficult since a nozzle of unknown  $\omega$  and  $M_{CD} - M_B$  had to be found. Inasmuch as it was impractical to compute a complete characteristic network for each combination of parameters, an empirical equation was found based upon available contours of Ref. 5. This empirical equation for the streamline AD is

$$y = \sqrt{F^2 + G(x - x_D)^3} + y_D - F \quad (29)$$

where

$$F = g \left( \frac{f - 1.5 g}{f - 3 g} \right)$$

$$G = \frac{f g^2}{(f - 3 g) x_{AD}^3}$$

$$f = x_{AD} \tan \omega$$

$$g = y_D - y_A$$

This equation satisfies most of the same end conditions as the streamline AD, i. e., the ordinate and slope at point A are those of the radial-flow region, the ordinate at point D is obtained from the area ratio, and the slope and second derivative are zero. The second derivative at point A and the third derivative at point D differ from those of the streamline AD, but, as shown in Fig. 5, the empirical curve is sufficiently close to the streamline for preliminary engineering purposes.

After many trials, it was found that the parameters for the Mach 10 contour should be  $\omega = 8.3993$  deg and  $M_{CD} = M_B = 1.3096$ . The characteristic solution for the streamline AD was computed by the Digital Computation Branch of the Aeronautical Research Laboratory at Wright-Patterson AFB who also computed the contours of Ref. 5. In addition to the coordinates and stream angles along the contour, the Mach angles were also furnished so that the Mach number distribution could be determined to facilitate the computation of the boundary-layer correction. A comparison of this correct Mach number distribution with the empirical one obtained by Eq. (28) is shown in Fig. 6. After the true ordinates and Mach number distribution were received, the final physical contour was calculated. The final pertinent dimensions are given in Table 1 and the coordinates in Table 3.

Since the operating pressures and temperatures of the Mach 10 Tunnel (C) are sufficiently high so that real gas effects must be taken into account in determining the throat area, the real gas area ratio was computed by means of Ref. 10 to be 2 percent greater than the ideal gas ratio for Mach 10 and 9 percent greater for Mach 12.

In the final stress and thermal analysis of the Mach 10 throat section (Ref. 4), it was found desirable to provide an expansion joint at a station on the subsonic contour where the Mach number was approximately 0.1. The same axial station was selected for a similar joint in the Mach 12 throat, and the ratio of throat-radius-of-curvature to throat radius was increased from 35 to 38.179. The Mach 12 throat, however, has not as

yet been built. The coordinates of the Mach 12 throat are given in Table 4 together with the inviscid nozzle coordinates. The inviscid contours for both the Mach 10 and Mach 12 nozzles are compared in Fig. 7 with the physical contour for Mach 10.

### 3.0 FABRICATION

Although the mechanical design of the Mach 10 Tunnel is presented in detail in Ref. 3, the fabrication of the Mach 8 and 10 nozzles is briefly described because of its effect on the Mach number distributions in the test regions.

As shown in Figs. 1 and 2, the throat sections are encased in heavy shells designed to withstand the maximum stagnation pressures. Downstream of the throat sections, the nozzles were fabricated in sections to facilitate machining the contours. Each section has double walls for the water cooling system and is flanged to mate with the adjacent sections. The Mach 8 Tunnel (B) has six sections between the throat and the test section with one section upstream of the inflection point and the other five downstream. The Mach 10 Tunnel also has six sections all of which are downstream of the inflection point since the throat section was made long enough to include both the subsonic and supersonic contours.

In axisymmetric nozzles, a circumferential disturbance to the flow is focused on the axis of the nozzle and its effect on flow uniformity is thereby magnified in comparison with the effect of a similar disturbance in a two-dimensional nozzle. It was therefore imperative that close tolerances be maintained in the machining of the nozzle contours and that the flanged joints be accurately aligned. In most cases the steps in the contour at the joints are within 0.002 in., and all the steps are within 0.005 in. Such tolerances are believed to be acceptable in nozzles of this size. As indicated in Ref. 3, the tolerances were specified to be smaller at the upstream end where the nozzle diameter was smaller.

Upstream of each nozzle, the ducting, which forms the stilling chamber, contains a perforated cone for reducing transverse temperature variations and coarse screens for reducing transverse velocity variations. The Mach 8 Tunnel (B) also has fine screens for reducing the turbulence level. Such screens were initially installed in the Mach 10 Tunnel (C) but deteriorated so rapidly at the high stagnation temperature that they were removed. The stilling chamber for the Mach Tunnel (B) is 26 in. in diameter to produce a contraction ratio of about 67:1. For the Mach 10 Tunnel (C), the 12-in. -diam stilling chamber gives a contraction ratio of about 47:1. At the downstream end of each stilling chamber is an instrumentation ring through which chromel-alumel

thermocouple probes are inserted at various distances to measure the distribution of stagnation temperature. The stagnation pressure is also measured at this location.

## 4.0 CALIBRATION

### 4.1 STAGNATION TEMPERATURE DISTRIBUTION

#### 4.1.1 Mach 8 Tunnel (B)

A typical distribution of the stagnation temperature measured at the instrumentation ring is given in Fig. 8. The values at the locations measured vary from 809 to 843°F. If the outermost measurements are ignored, the temperature is uniform within about  $\pm 7$  deg; this variation approaches the accuracy of the thermocouples which is  $\pm 6$  deg. There is no indication of striation; in fact, the lowest temperature measured was at the top.

#### 4.1.2 Mach 10 Tunnel (C)

A typical distribution of the stagnation temperature measured at the instrumentation ring is given in Fig. 9. In this case the measured values vary from 1437 to 1509°F. Again there is no evidence of striation even though the lowest value is at the bottom. If the top and bottom values are ignored, the temperature is uniform within  $\pm 15$  deg. At these temperatures, the accuracy of the thermocouple junctions is about  $\pm 11$  deg neglecting unknown aging effects of chromel-alumel thermocouples which occur in the temperature range of 1000 to 1200°F.

### 4.2 MACH NUMBER DISTRIBUTION

#### 4.2.1 Mach 8 Tunnel (B)

The Mach number distribution in the test region was determined by means of surveys with rakes of pitot tubes. The main calibration was made with a rake of 13 pitot tubes spaced 3 in. apart. The rake was mounted on a probe support actuated by a hydraulic cylinder to survey from about 43 in. ahead to 47 in. behind the center of model rotation. The rake was mounted vertically, horizontally, and at angles at  $\pm 45$  deg. Thus a cylindrical section that was 36 in. in diameter and 90 in. long was surveyed. Because of the time required to install and remove this probe support, a smaller rake, mounted on the regular model support,

has been used to check the distribution periodically. The axial travel of this smaller rake was limited to about 30 in. The pitot pressures were measured by means of transducers and the Mach number obtained by assuming isentropic expansion of the flow from the stilling chamber to the test section.

A typical result of the calibration is shown in Fig. 10. The center-line distribution is uniform within about  $\pm 1$  percent in Mach number, whereas off-center the flow is uniform to about  $\pm 0.3$  percent. The distributions in the various planes through the axis were essentially identical, indicating that the flow was axisymmetric as expected. At low pressure levels the distribution is somewhat more uniform than at the higher pressure levels. Furthermore, because of changes in boundary-layer thickness caused by changes in pressure level, the average Mach number is a function of pressure level and approximately follows the empirical relation

$$M = 8.125 - \frac{30}{p_o + 120} \quad (30)$$

where the stagnation pressure  $p_o$  is measured in psia. There is a slight mean axial gradient on the order of 0.01 Mach number per foot, although local gradients on the centerline exceed this value considerably.

At irregular intervals since the original calibration, check calibrations have been made. In September 1960, one such check showed a peak in the Mach number distribution about 13 in. ahead of the center of rotation followed by a dip about 4 in. further downstream. The difference in Mach number at these two points was about 0.3, which was about twice the deviation found originally. Since the tunnel was fabricated in flanged sections with the first joint only 5.31 in. downstream of the throat and the second joint at the inflection point about 21.90 in. downstream of the throat, it was suspected that the tunnel sections were out of line. To check the effect of disturbances created at these joints, 0.063-in. - thick shims were installed, one at a time, between the flanges. Because of the slope at these points, the shims formed forward-facing steps with a height of 0.013 in. These steps produced no significant change in the calibration over the 30-in. range covered by the surveys, as shown in Fig. 11. Based on investigations to date relative to the source of the flow disturbances, it is believed that a larger radius of curvature at the throat would produce more nearly uniform flow.

The effects of the centerline Mach number variations shown in Fig. 11 on the overall forces on models have been found to be negligible. Furthermore, the effects on pressure distributions of sharp-nosed bodies have also been found to be quite small. On the other hand, such variations have

an appreciable effect on the heat transfer and pressure distributions of blunt-nosed bodies. Figure 12 shows the pressure distributions measured on a 5.8-in. -diam hemisphere-cylinder model located at two positions on the axis of the Mach 8 Tunnel (B). With the nose located at approximately station 56 (about 9 in. upstream of the center of model rotation) where the centerline Mach number was a minimum, the stagnation point pressure was high corresponding to the low Mach number, and the pressure gradient near the stagnation point was relatively high. When the model was moved downstream about 18 in. where the centerline Mach number was more nearly constant, a normal pressure distribution was obtained. The difference in pressure distribution is limited to the subsonic region on the hemisphere since the distributions are essentially identical for azimuth angles greater than about 45 deg. These data indicate that, until the nozzle flow is improved, care must be taken to locate models in a suitable position.

#### 4.2.2 Mach 10 Tunnel (C)

The calibration probe support in the Mach 10 Tunnel (C) is permanently mounted in the diffuser as shown in Fig. 2. It can be used in the position shown or it can be extended 50 in. forward as described in Ref. 3. The travel of the probe in either position is 72 in. As used in the calibration, the conical nose was replaced by the same 36-in. -span rake of pitot tubes used at Mach 8. Isentropic flow was again assumed from the stilling chamber to the test section, but in this case, because of the higher stagnation pressure and temperature, the measured pressure ratio was corrected for real gas effects. The maximum correction was on the order of 2 percent.

A typical result of the calibration is shown in Fig. 13. The flow was again found to be truly axisymmetric. The centerline distribution is uniform within about  $\pm 0.5$  percent in Mach number, whereas off-center the flow is uniform to about  $\pm 0.2$  percent. The improved flow, relative to that found at Mach 8, is attributed to the much larger ratio of throat-radius-of-curvature to throat radius and/or the lower cone angle. The average Mach number is again a function of pressure level and approximately follows the empirical relation

$$M = 10.250 - \frac{150}{p_o + 500} \quad (31)$$

where the stagnation pressure  $p_o$  is measured in psia. Again there is a slight mean axial gradient on the order of 0.01 Mach number per foot.

### 4.3 FLOW ANGULARITY SURVEY

Flow angularity surveys were attempted only in the Mach 8 Tunnel (B). Even there, the hydraulically operated piston was found to be insufficiently rigid for accurate measurements since the geometric angle would change from one end of the probe travel to the other and the window area was too small to align the probe optically except in a limited region. Therefore, a single probe was mounted on a sting which allowed the probe to be offset from the tunnel axis. Rolling the sting caused the probe to move in a circular path around the tunnel axis. The length of the sting limited the survey to one axial position near the plane containing the center of model rotation. This plane was also near the center of the window so that optical equipment could be used for accurate alignment. Continuous monitoring of the alignment was necessary while the tunnel was operating to correct for thermal distortions of the equipment caused by high stagnation temperature.

A shadowgram of the flow about the probe is shown in Fig. 14. The probe was conical with a 10-deg half-angle. Four pitot tubes were mounted 90 deg apart near the rear of the cone in such a manner that they were outside of the cone boundary layer but inside of the bow shock wave. Pitot tubes were used rather than static orifices on the cone surface to increase the sensitivity to angle of attack and to reduce the time required for the pressures to stabilize. The pressure differences between oppositely mounted probes were measured, as well as the pitot pressure at the nose of the cone. The probe was calibrated by pitching it in both erect and inverted positions.

The survey indicated that the flow at this station in the tunnel was diverging at a rate of approximately 0.4 deg per foot of radial distance from the tunnel axis. According to the simple theory of radial diverging flow,

$$\frac{\alpha}{y} = \frac{(M^2 - 1)}{(\gamma - 1) M \left( M^2 + \frac{2}{\gamma - 1} \right)} \frac{dM}{dx} \quad (32)$$

a divergence of this amount corresponds to a Mach number gradient of 0.025 per foot, which is over twice the average measured gradient. Therefore it is believed that the measured flow angles represent local conditions and that the average divergence is probably less than 0.2 deg (0.16 theoretically) per radial foot.

Because the difficulties of measuring flow angularity in the Mach 10 Tunnel (C) would be even greater because of the higher stagnation temperature, it was not attempted. The theoretical divergence at Mach 10 corresponding to a gradient of 0.01 Mach number per foot is 0.135 deg per radial foot.

#### 4.4 BOUNDARY-LAYER SURVEY

##### 4.4.1 Mach 8 Tunnel (B)

The boundary layer in the tunnel was surveyed at a station 13.3 in. upstream of the center of model rotation (245.0 in. downstream of the throat). A pitot tube and a stagnation temperature probe were used in the survey. The boundary-layer thickness was found to vary from about 7 in. at a stagnation pressure of 100 psia to about 5.5 in. at 550 psia. The corresponding displacement thickness varied from 2.7 to 2.3 in.

##### 4.4.2 Mach 10 Tunnel (C)

The boundary layer in the tunnel was surveyed at a station 3.8 in. downstream of the beginning of the test section (299.2 in. downstream of the throat). The instrumentation used was similar to that used at Mach 8. The boundary-layer thickness was found to vary from about 11 in. at a stagnation pressure of 200 psia to about 8.2 in. at 1800 psia. The corresponding displacement thickness varied from 4.3 to 3.1 in.

#### 4.5 DIFFUSER PERFORMANCE

##### 4.5.1 Mach 8 Tunnel (B)

Downstream of the 50-in. -diam, 6-ft-long model support section is a diffuser duct (see Fig. 1) which is also 50 in. in diameter for a distance of 22.5 ft, after which a 5-ft-long section makes a transition to a 40 by 43.25-in. rectangular section to match an existing duct which expands to 7 ft in diameter at the entrance to the cooler. The rectangular section therefore represents the second minimum of the diffuser and has a cross-sectional area of 88 percent of the test section area.

Pressure ratios of 180:1 to 240:1 are required to start the tunnel, depending upon the model configuration. These values are about 150 to 200 percent of normal-shock ratio. The size of models which will allow starting of the tunnel varies greatly with the type of model. Flat plate models, normal to the airstream, can have a cross-sectional area of about 50 sq in. Delta wing models with a planform area of about 150 sq in. will allow starting at 30 deg angle of attack (75 sq in. frontal area), after which the model can be pitched to 60 deg. Axisymmetric models with flares up to 16 in. in diameter will allow starting if the nose section is small enough.

Attempts were made to improve the diffuser performance with a central body and/or converging-diverging fairings inside the diffuser duct. All such attempts required reducing the size of the models or limiting the maximum angle of attack, possibly because of the presence of the rectangular section at the end of the constant diameter duct. Since the pressure ratio available from the compressor plant was more than sufficient, the central body and fairings were removed.

#### 4.5.2 Mach 10 Tunnel (C)

The test section (Fig. 2) is conical for 54 in. (48.5-in. diameter to 50-in. diameter), after which it is cylindrical (50-in. diameter) for 72 in. Following the test section, the diffuser duct is 50 in. in diameter for a length of 26 ft, after which it expands at a 6-deg total angle to 120 in. in diameter at the entrance to the cooler. The 22-ft-long calibration probe housing is 14 in. in diameter (cross-sectional area about 6 percent of diffuser area), dropping to 10 in. in diameter at the downstream end. This probe housing may be considered to be a centerbody diffuser but is not believed to materially affect the starting pressure ratio.

A pressure ratio of about 360:1 is required to start the tunnel which, of course, is with the model and its support retracted into the test section tank. This ratio is only about 110 percent of normal-shock ratio. This low value, relative to the Mach 8 requirements, is attributed to the lower expansion angle and the absence of the restriction present in the Mach 8 diffuser duct. The fact that the model is retracted in the Mach 10 Tunnel (C) is, of course, a factor in the starting-pressure requirement. However, in the Mach 8 Tunnel (B) during initial calibration, the probe support housing was approximately the same size as that in the Mach 10 Tunnel (C) and the higher pressure ratio was required. In fact, the Mach 8 Tunnel (B) would not start at all unless the calibration probe was moved forward into the test section.

Although the tunnel is normally started with the doors closed between the test section and the test section tank (Fig. 2), opening the doors has no apparent effect on the pressure ratio required to start or run the Mach 10 Tunnel (C). This fact was established before construction of the tunnel by mounting a chamber of corresponding size on the side of a 12 x 12-in., hypersonic blow-down-type tunnel and observing its effect on the operation of that tunnel.

The size of models which can be injected into the test section after the tunnel is started depends upon the type of the mode. A flat-plate,

70-deg delta wing with a planform area of 100 sq in. can be injected at an angle of attack of 90 deg (normal to the flow). A delta wing model with a planform area of about 125 sq in. can be injected at an angle of attack of -50 deg, whereas the maximum positive angle of attack is about 20 deg. After injection a delta wing model with a planform area of about 150 sq in. can be pitched to an angle of attack of 60 deg. Large models of other shapes seem to inject better if inverted so that the aerodynamic load is downward. This phenomenon appears to be associated with the fact that the test section is open to the tank during injection and blockage occurs only if an appreciable amount of the airflow is deflected into the tank.

### 5.0 CONCLUDING REMARKS

The aerodynamic design has been described for two 50-in. -diam, axisymmetric contoured nozzles for which calibration data have been obtained. In the Mach 8 Tunnel (B), the flow on the centerline is uniform within about  $\pm 1$  percent in Mach number and off-center within about  $\pm 0.3$  percent. In the Mach 10 Tunnel (C), the centerline distribution is uniform within about  $\pm 0.5$  percent in Mach number, whereas off-center the flow is uniform to about  $\pm 0.2$  percent. Both tunnels have a slight mean axial gradient on the order of 0.01 Mach number per foot.

The better results obtained at Mach 10 are attributed to the lower expansion angle and larger radius of curvature at the throat than those incorporated in the Mach 8 design. As part of a general maintenance and modernization program for the Mach 8 Tunnel (B), plans are being made to replace the throat section with one having a larger radius of curvature. The lower expansion angle at Mach 10 is also believed to be a factor in the lower relative pressure ratio required for starting.

The two VKF 50-in. hypersonic tunnels are the largest of their type known to be in operation and have proven to be extremely useful for research and development testing.

### REFERENCES

1. Lukasiewicz, J. "Experimental Investigation of Hypervelocity Flight." Advances in Aeronautical Sciences, 1, Pergamon Press, 1939, pp. 127-186 (First International Congress of Aeronautical Sciences, Madrid, Spain, Sept. 1958).

2. Test Facilities Handbook, (Fourth Edition). "von Kármán Gas Dynamics Facility, Vol. 4." Arnold Engineering Development Center, July 1962.
3. Howard, Charles M. "Mechanical Design of the 50-Inch Mach 10-12 Tunnel (C)." AEDC-TDR-62-229, April 1963.
4. Sherman, R. and Cook, J. P. "Stress and Thermal Analysis of the Throat Sections - 50-Inch Mach 10 and 12 Tunnel (C)." AEDC-TDR-62-231, February 1963.
5. Cresci, Robert J. "Tabulation of Coordinates for Hypersonic Axisymmetric Nozzles Part 1 - Analysis and Coordinates for Test Section Mach Numbers of 8, 12, and 20." WADC Technical Note 58-300 Part 1, October 1958.
6. Yu, Ying-Nien. "A Summary of Design Techniques for Axisymmetric Hypersonic Wind Tunnels." AGARDograph 35, November 1958.
7. Foelsch, K. "The Analytical Design of an Axially Symmetric Laval Nozzle for a Parallel and Uniform Jet." Journal of the Aeronautical Sciences, Vol. 16, 1949.
8. Sivells, James C. and Payne, Robert G. "A Method of Calculating Turbulent-Boundary-Layer Growth at Hypersonic Mach Numbers." AEDC-TR-59-3, March 1959.
9. Durand, J. A. and Potter, J. Leith. "Calculation of Thicknesses of Laminar Boundary Layer in Axisymmetric Nozzles with Low-Density, Hypervelocity Flows." AEDC-TN-61-146, December 1961.
10. Randall, R. E. "Thermodynamic Properties of Air; Tables and Graphs Derived from the Beattie-Bridgeman Equation of State Assuming Variable Specific Heats." AEDC-TR-57-8, August 1957.



TABLE 1  
PERTINENT DIMENSIONS OF AXISYMMETRIC NOZZLES

$M_{CD}$	8	10	12
$M_B$	7.8	8.6904	11.8
$\omega$ (deg)	12	8.3993	8
$\omega'$ (deg)	12.517	9.065	9.065
$M_A$	4.4066	5.5271	6.9100
$r_1$ (in.)	7.4565	6.1282	3.8797
$x_A/r_1$	3.8256	6.0685	9.8165
$y_A/r_1$	0.8131	0.8965	1.3796
$x_B/r_1$	13.0155	16.6777	34.3132
$x_{BC}/r_1$	2.1979	14.3347	4.0799
$x_{CD}/r_1$	22.8791	33.7369	59.5997
$y_D/r_1$	2.8825	3.3907	4.9840
$x_E$ (in.)	-19.692	-20.571	-18.704
$Y^*$ (in.)	1.584	0.873	0.560
$x_{EA}$ (in.)	41.591	54.000	54.000
$Y_A$ (in.)	6.183	5.713	5.713
$x_{EB}$ (in.)	110.115	119.012	149.040
(in.)	126.504	206.858	164.869
$x_{ED}$ (in.)	297.102	413.605	395.253

TABLE 2  
COORDINATES OF MACH 8 CONTOUR

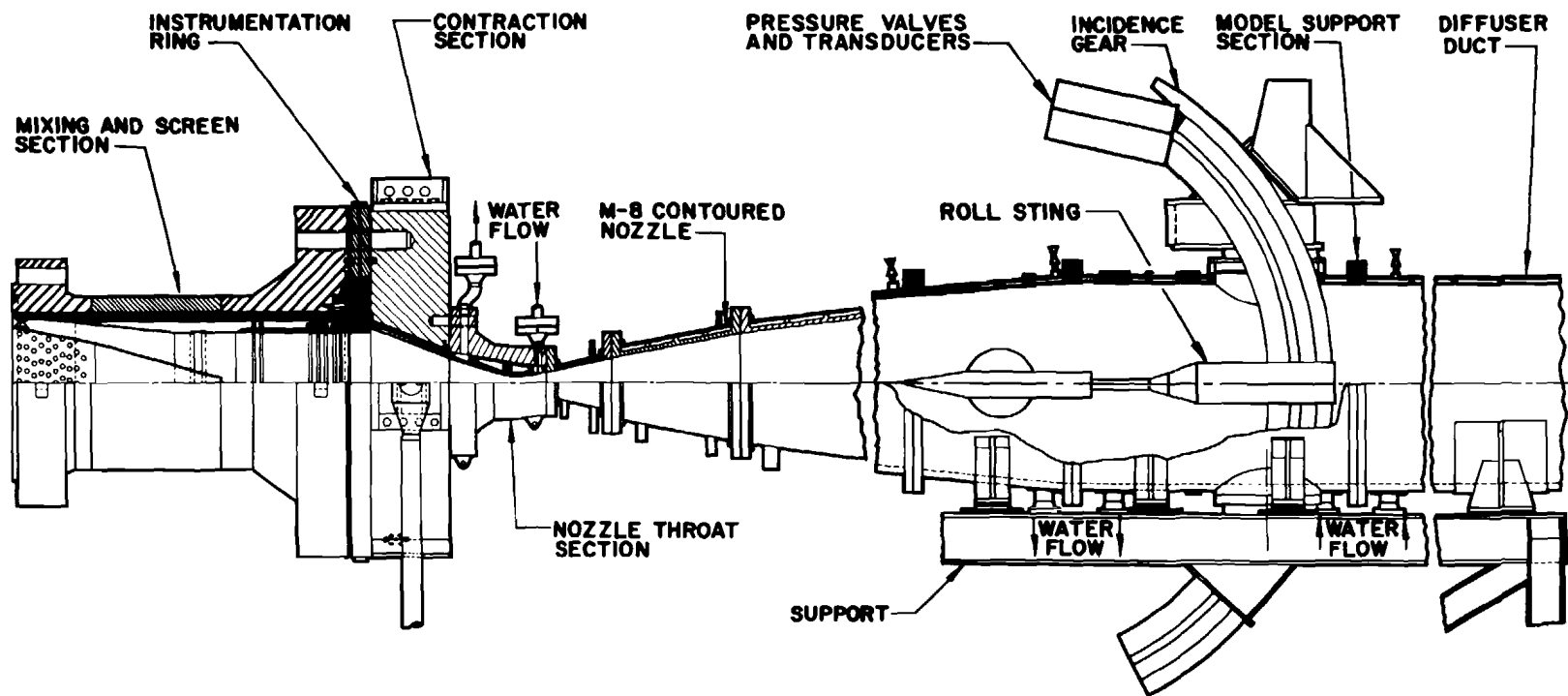
X - X <sub>E</sub>	y	Y	X - X <sub>E</sub>	y	Y
0		6.000	111.501	16.051	16.940
15.899		2.189	111.032	16.271	17.192
17.000		1.933	116.593	16.488	17.441
18.000		1.738	119.184	16.700	17.686
19.000		1.612	121.803	16.907	17.927
19.400		1.589	124.452	17.110	18.164
19.600		1.585	127.129	17.308	18.397
19.692		1.584	129.835	17.501	18.626
19.800		1.585	132.569	17.690	18.849
20.000		1.590	135.332	17.874	19.070
21.000		1.680	138.122	18.054	19.286
22.000		1.848	140.941	18.229	19.498
23.586		2.186	143.787	18.399	19.706
41.591	6.063	6.183	146.662	18.564	19.910
42.609	6.280	6.409	149.562	18.724	20.110
44.132	6.602	6.745	152.491	18.880	20.305
45.831	6.955	7.116	155.446	19.031	20.495
47.313	7.259	7.433	158.428	19.177	20.682
48.857	7.568	7.757	161.436	19.318	20.862
50.441	7.880	8.083	164.471	19.454	21.039
52.060	8.190	8.410	167.532	19.586	21.212
53.674	8.495	8.731	170.618	19.713	21.382
55.302	8.796	9.048	173.730	19.835	21.548
56.929	9.089	9.357	176.868	19.952	21.708
58.577	9.380	9.664	180.030	20.065	21.865
60.275	9.671	9.973	183.217	20.173	22.017
62.001	9.963	10.282	186.429	20.276	22.163
63.773	10.255	10.592	189.665	20.375	22.306
65.584	10.546	10.902	192.924	20.469	22.444
67.433	10.836	11.212	196.208	20.559	22.578
69.319	11.124	11.520	199.514	20.644	22.708
71.242	11.411	11.828	202.844	20.724	22.834
73.199	11.696	12.134	206.196	20.800	22.956
75.192	11.978	12.438	209.572	20.872	23.074
77.220	12.259	12.741	212.966	20.939	23.188
79.280	12.536	13.041	216.384	21.002	23.295
81.375	12.810	13.339	219.823	21.061	23.399
83.503	13.081	13.634	223.282	21.115	23.499
85.653	13.350	13.927	226.761	21.166	23.595
87.855	13.614	14.217	230.261	21.213	23.688
90.080	13.875	14.504	233.779	21.255	23.776
92.336	14.133	14.788	237.316	21.294	23.859
94.625	14.387	15.070	240.873	21.329	23.938
96.944	14.637	15.348	244.445	21.361	24.011
99.294	14.883	15.622	248.036	21.389	24.081
101.674	15.125	15.894	251.643	21.413	24.146
104.085	15.362	16.161	255.266	21.435	24.205
106.527	15.596	16.424	258.000	21.448	24.246
108.999	15.826	16.684	298.000		25.000

TABLE 3  
COORDINATES OF MACH 10 CONTOUR

X - X <sub>E</sub>	y	Y	X - X <sub>E</sub>	y	Y
0		6.000	106.426	12.120	12.983
11.793			108.964	12.368	13.262
14.000		1.601	114.144	12.857	13.812
16.000		1.239	119.472	13.336	14.358
18.000		.993	124.939	13.802	14.894
20.000		.879	130.543	14.255	15.421
20.250		.875	136.285	14.695	15.935
20.571		.873	142.155	15.120	16.438
20.750		.874	148.155	15.531	16.927
21.000		.877	154.288	15.927	17.405
22.000		.911	160.542	16.302	17.869
24.000		1.071	166.926	16.671	18.319
26.000		1.311	173.428	17.019	18.755
28.000		1.591	180.057	17.351	19.178
30.000		1.893	186.807	17.666	19.587
32.000		2.205	193.675	17.965	19.981
34.000		2.522	197.151	18.108	20.173
35.926		2.829	200.660	18.247	20.362
54.000	5.491	5.713	204.193	18.382	20.546
55.005	5.640	5.874	207.761	18.512	20.728
55.994	5.786	6.032	211.350	18.639	20.904
56.985	5.932	6.190	214.974	18.761	21.077
57.986	6.080	6.350	218.621	18.879	21.246
59.006	6.230	6.510	222.299	18.994	21.412
60.055	6.385	6.679	226.000	19.103	21.573
61.140	6.544	6.852	229.734	19.209	21.732
62.269	6.709	7.030	233.489	19.311	21.886
63.451	6.880	7.216	237.275	19.409	22.036
64.692	7.060	7.410	241.089	19.502	22.183
65.999	7.247	7.613	244.922	19.592	22.327
67.376	7.443	7.827	248.787	19.678	22.468
68.830	7.647	8.049	252.677	19.759	22.603
70.362	7.861	8.280	256.587	19.837	22.735
71.976	8.082	8.522	260.526	19.911	22.863
73.671	8.313	8.772	264.485	19.981	22.989
75.447	8.550	9.031	268.472	20.047	23.110
77.301	8.794	9.298	272.483	20.110	23.227
79.230	9.043	9.571	276.512	20.169	23.340
81.227	9.297	9.849	280.568	20.224	23.451
83.285	9.554	10.131	284.647	20.276	23.557
85.394	9.812	10.416	288.743	20.324	23.661
87.556	10.071	10.701	292.864	20.369	23.758
89.766	10.330	10.987	296.970	20.410	23.853
92.022	10.590	11.273	301.129	20.448	23.945
94.321	10.848	11.561	305.286	20.483	24.036
96.659	11.105	11.846	309.480	20.516	24.124
99.042	11.362	12.132	313.679	20.545	24.207
101.464	11.616	12.418	316.000		24.250
103.926	11.869	12.701	370.000		25.000

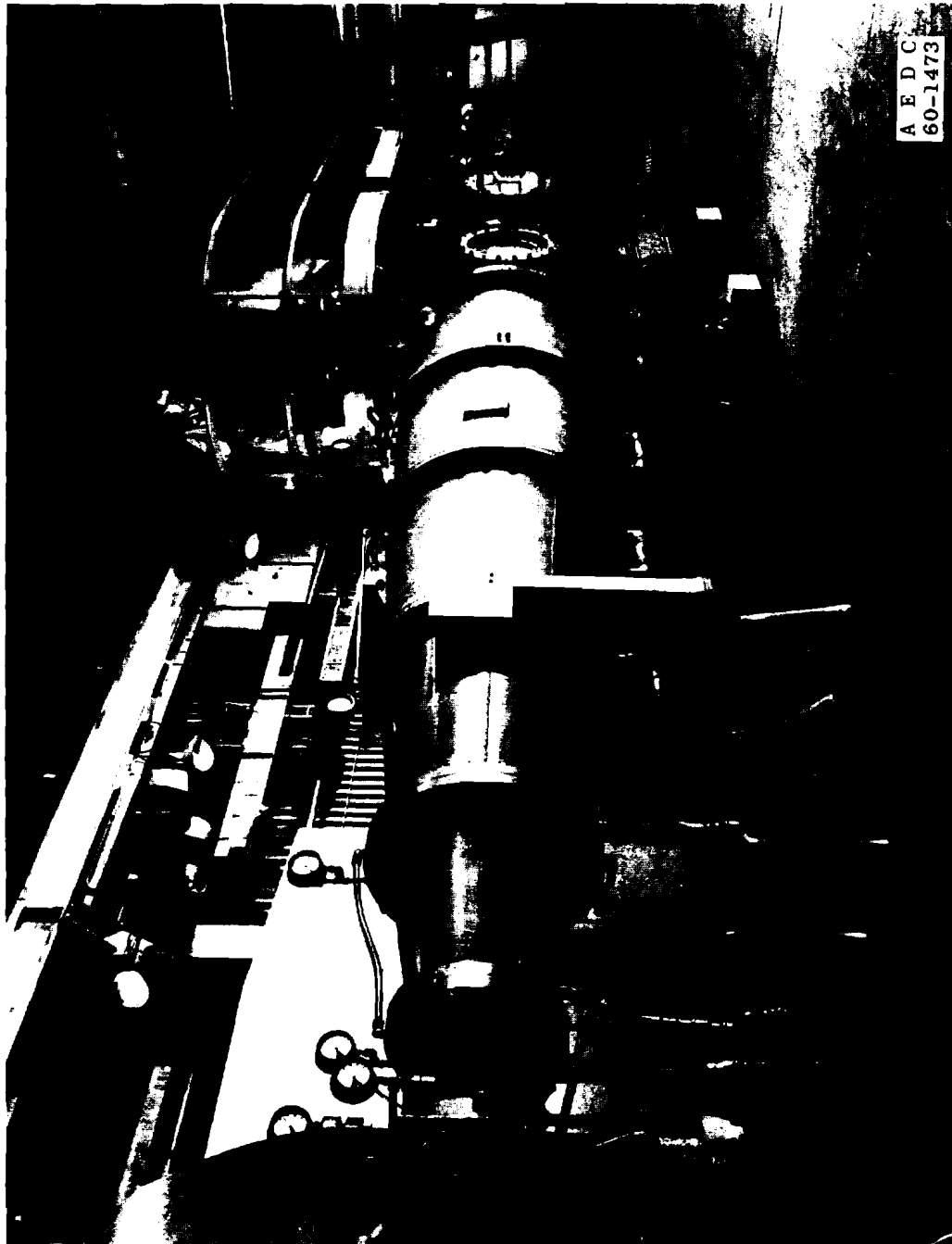
TABLE 4  
COORDINATES OF MACH 12 CONTOUR

X - X <sub>E</sub>	y	Y	X - X <sub>E</sub>	y	Y
0		6.000	115.696		12.080
11.793		1.538	120.783		12.480
14.000		1.034	125.990		12.871
16.000		.723	131.313		13.252
18.000		.572	136.756		13.622
18.500		.561	142.312		13.982
18.704		.560	147.985		14.331
19.000		.562	153.770		14.669
20.000		.598	159.671		14.995
22.000		.773	165.681		15.310
24.000		1.023	171.804		15.612
26.000		1.306	178.035		15.903
28.000		1.604	184.370		16.182
30.000		1.909	190.819		16.448
32.000		2.220	197.372		16.703
34.000		2.533	200.685		16.825
36.000		2.848	204.030		16.945
38.000		3.165	207.398		17.061
42.000		3.800	210.793		17.174
46.000		4.437	214.211		17.284
50.000		5.075	217.656		17.391
54.000	5.353	5.713	221.129		17.495
55.325	5.539		224.621		17.596
57.075	5.784		228.144		17.694
58.662	6.003		231.686		17.789
60.198	6.213		235.259		17.880
61.797	6.428		238.848		17.969
63.438	6.646		242.468		18.054
65.110	6.865		246.111		18.137
66.798	7.083		249.778		18.216
68.505	7.299		253.464		18.293
70.247	7.517		257.177		18.366
72.036	7.737		260.913		18.437
73.871	7.958		264.673		18.504
75.749	8.180		268.452		18.568
77.665	8.403		272.254		18.630
79.621	8.626		276.080		18.689
81.619	8.850		279.925		18.745
83.652	9.074		283.793		18.798
85.720	9.296		287.681		18.849
87.827	9.519		291.592		18.896
89.969	9.740		295.522		18.941
92.141	9.960		299.472		18.983
94.353	10.180		303.441		19.022
96.596	10.398		307.429		19.059
98.873	10.615		311.437		19.094
101.182	10.830		315.461		19.126
105.896	11.254		316.000		
110.734	11.672		370.000		
					24.250
					25.000



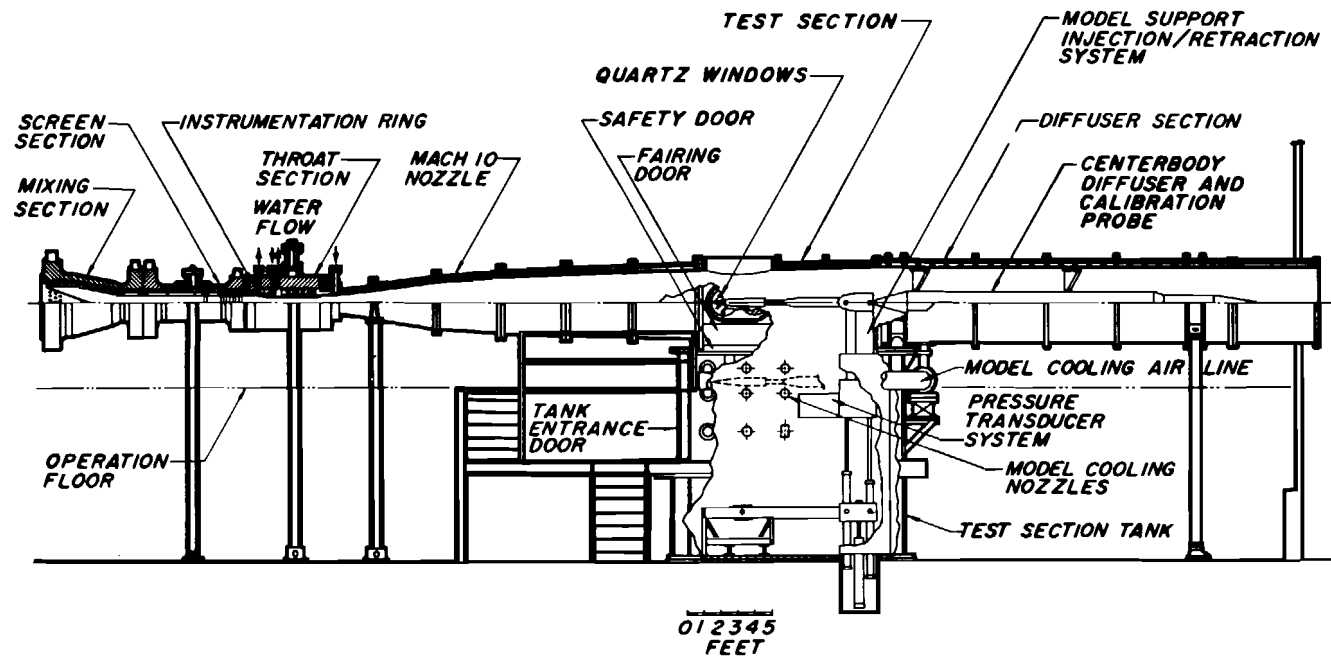
a. General Arrangement

Fig. 1 The 50-Inch Mach 8 Tunnel (B)



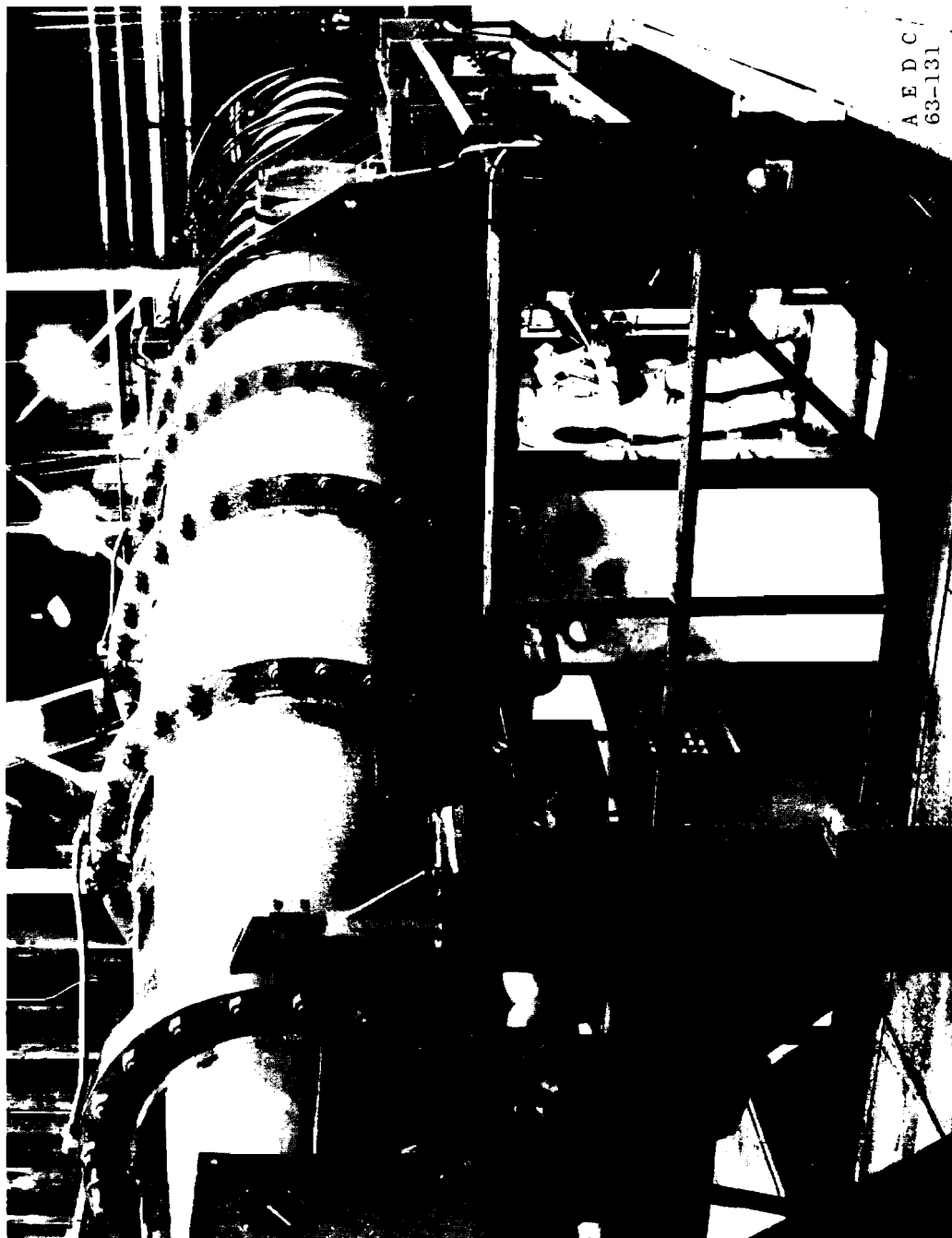
b. View Looking Downstream

Fig. 1 Concluded



a. General Arrangement

Fig. 2 The 50-Inch Mach 10 Tunnel (C)



b. View Looking Downstream

Fig. 2 Concluded

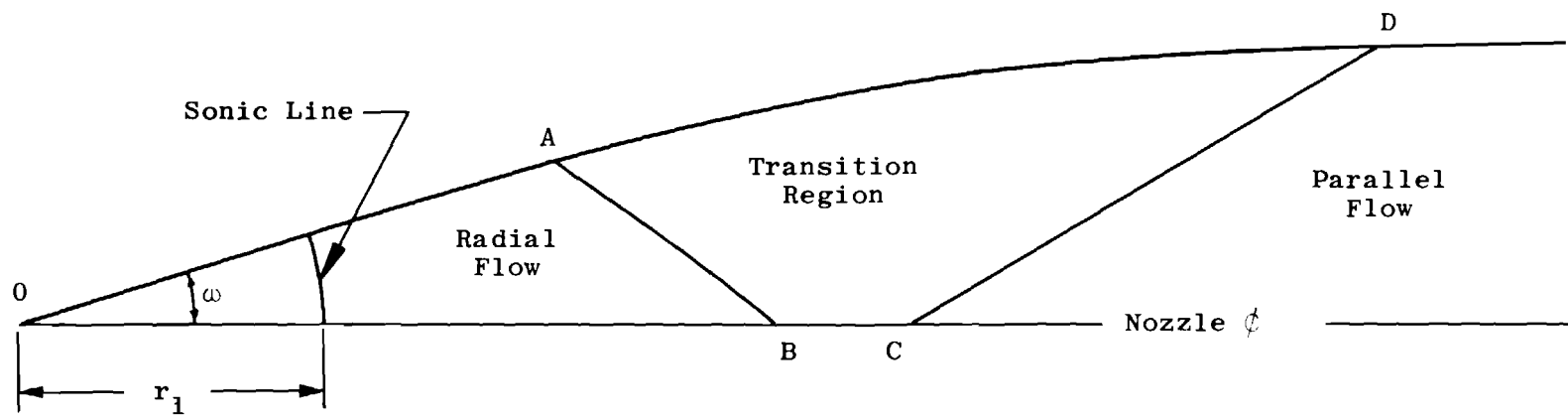


Fig. 3 Downstream Inviscid Contour

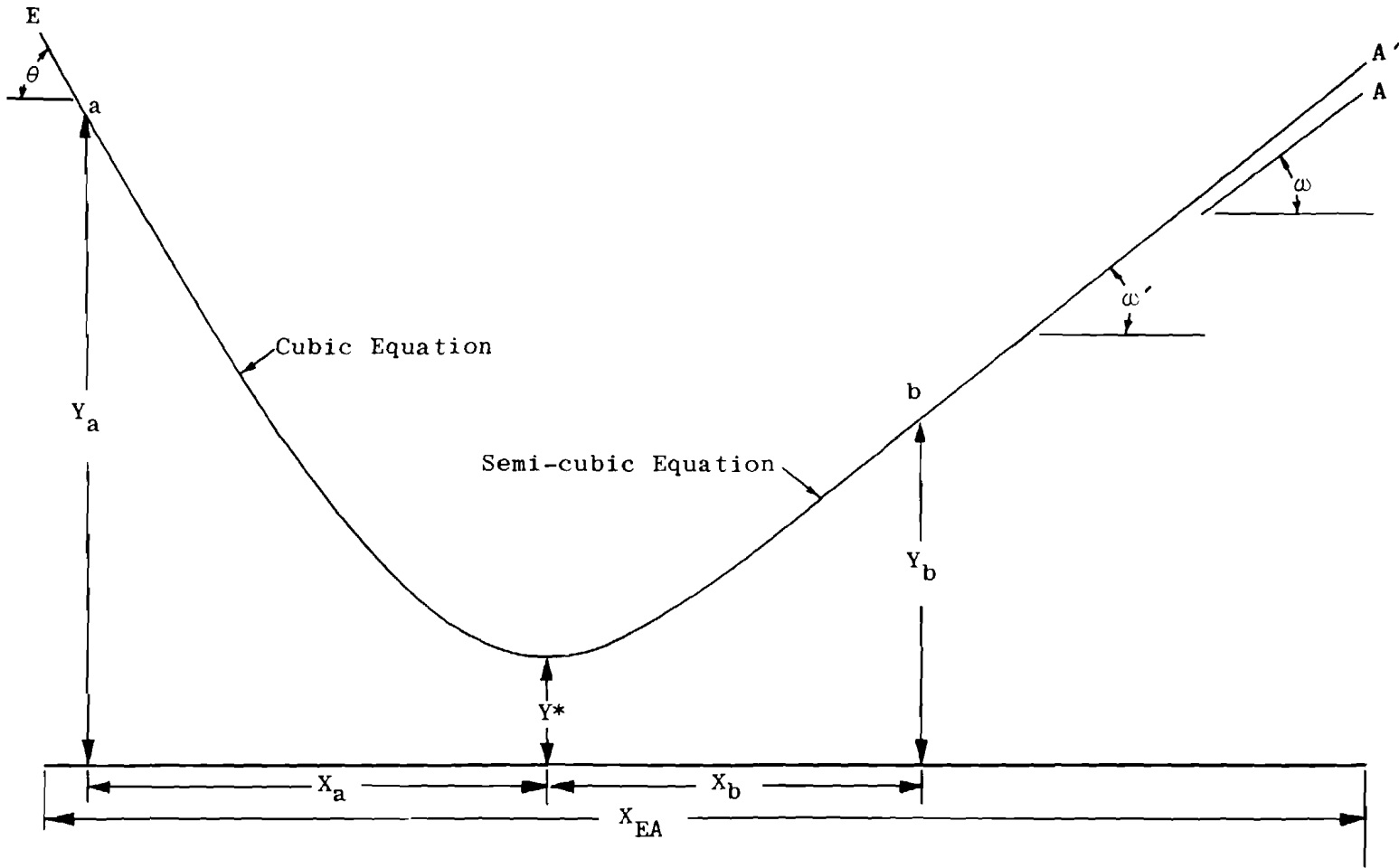


Fig. 4 Throat Contour

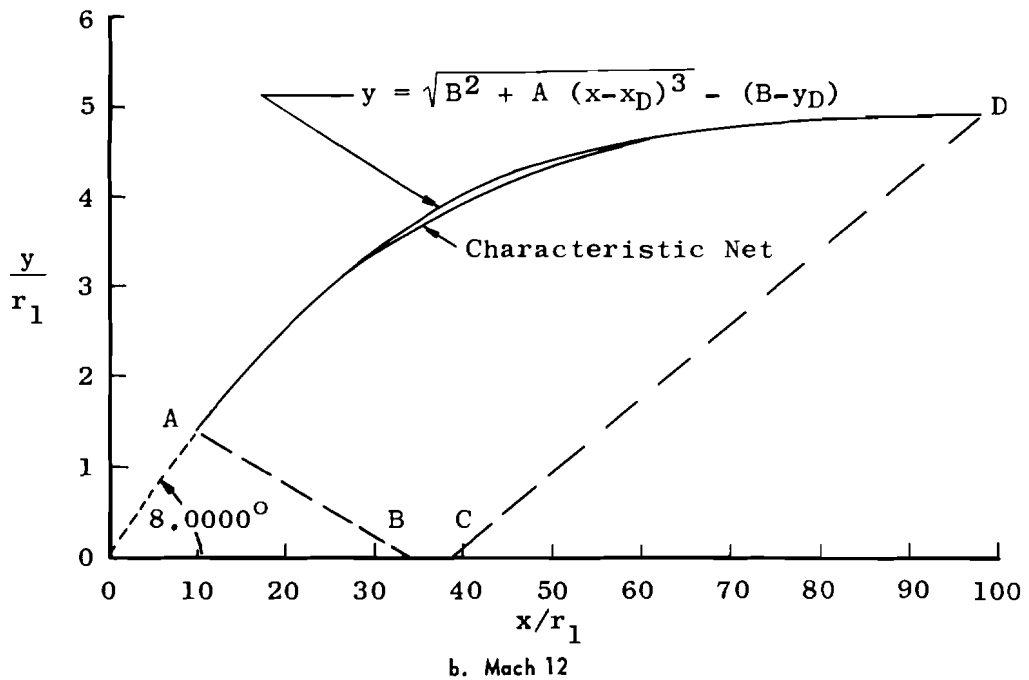
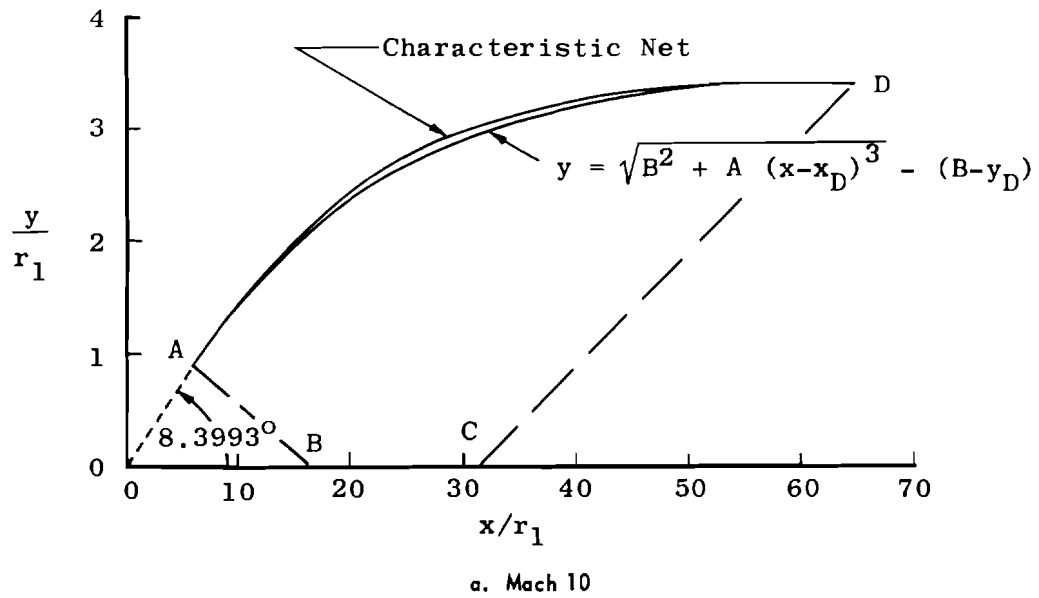


Fig. 5 Comparison of Theoretical and Empirical Inviscid Contours

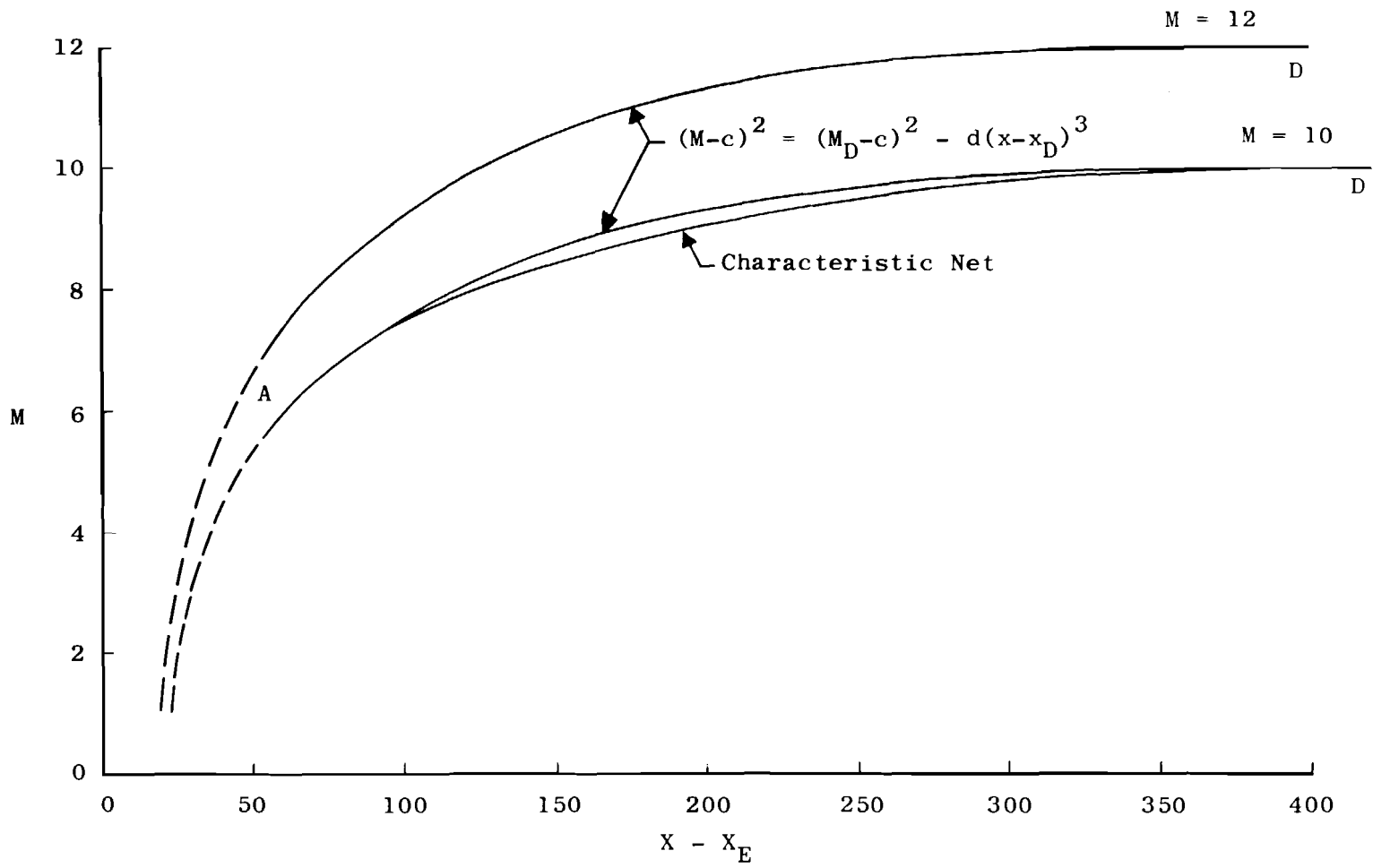


Fig. 6 Comparison of Theoretical and Empirical Mach Number Distribution

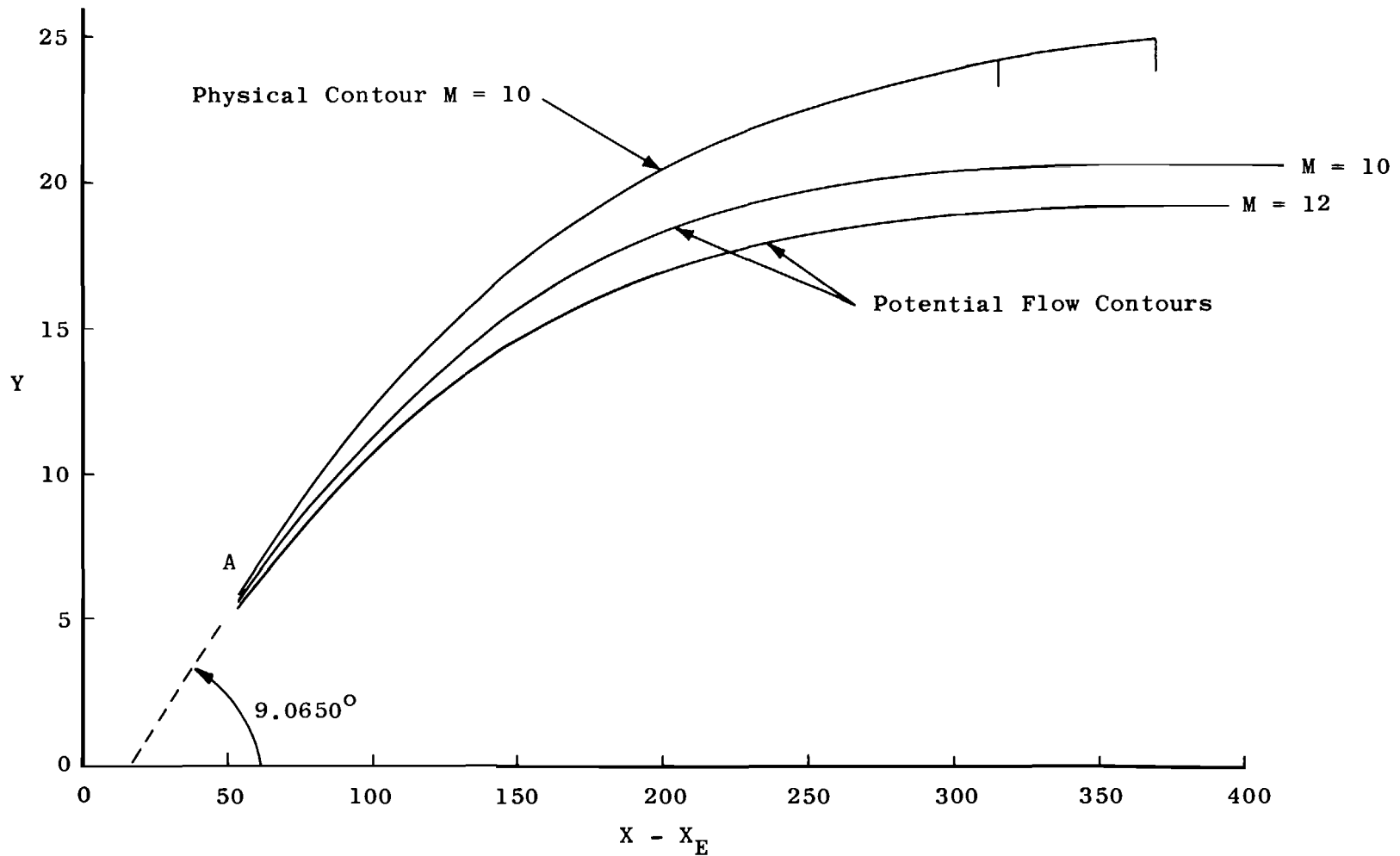
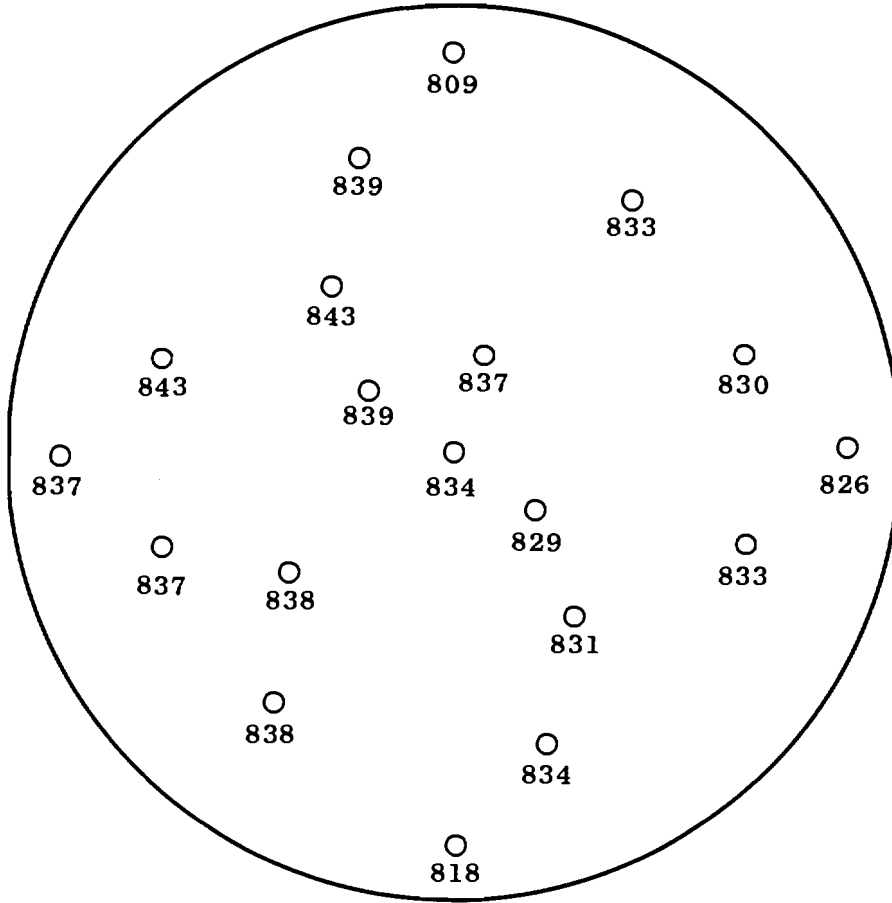
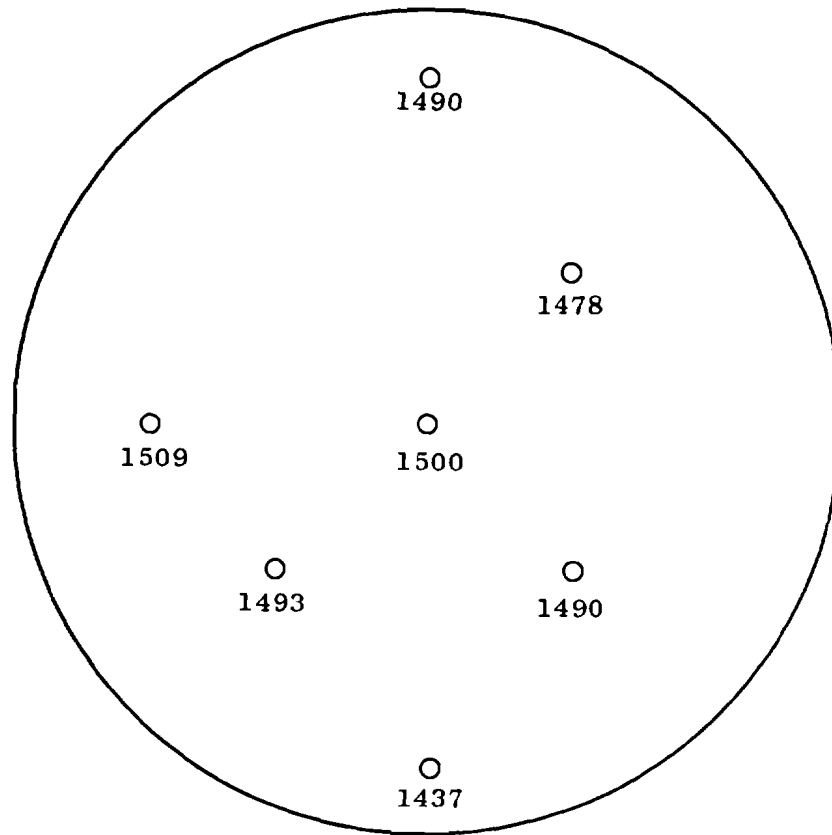


Fig. 7 Inviscid Contours for the Mach 10 and 12 Nozzles Compared to the Physical Contour for Mach 10



**Fig. 8 Air Temperatures Measured in the Mach 8 Tunnel (B) Instrumentation Ring as Viewed Looking Downstream; Stagnation Pressure = 500 psia; Inside Diameter of Instrumentation Ring = 26 in.; Temperatures in °F**



**Fig. 9 Air Temperatures Measured in the Mach 10 Tunnel (C) Instrumentation Ring as Viewed Looking Downstream; Stagnation Pressure = 1600 psia; Inside Diameter of Instrumentation Ring = 12 in.; Temperatures in °F**

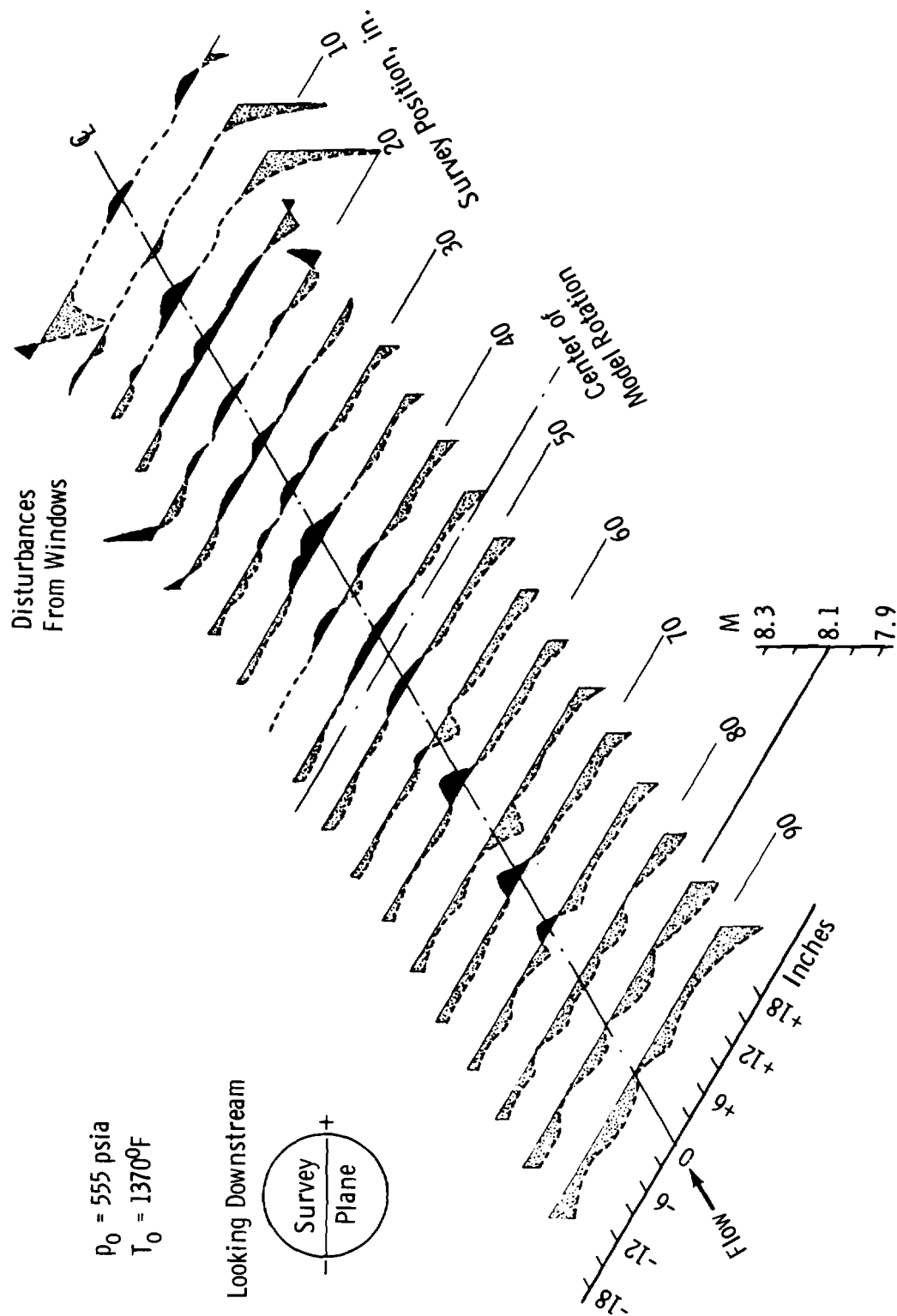


Fig. 10 Mach Number Distribution in the Mach 8 Tunnel (B)

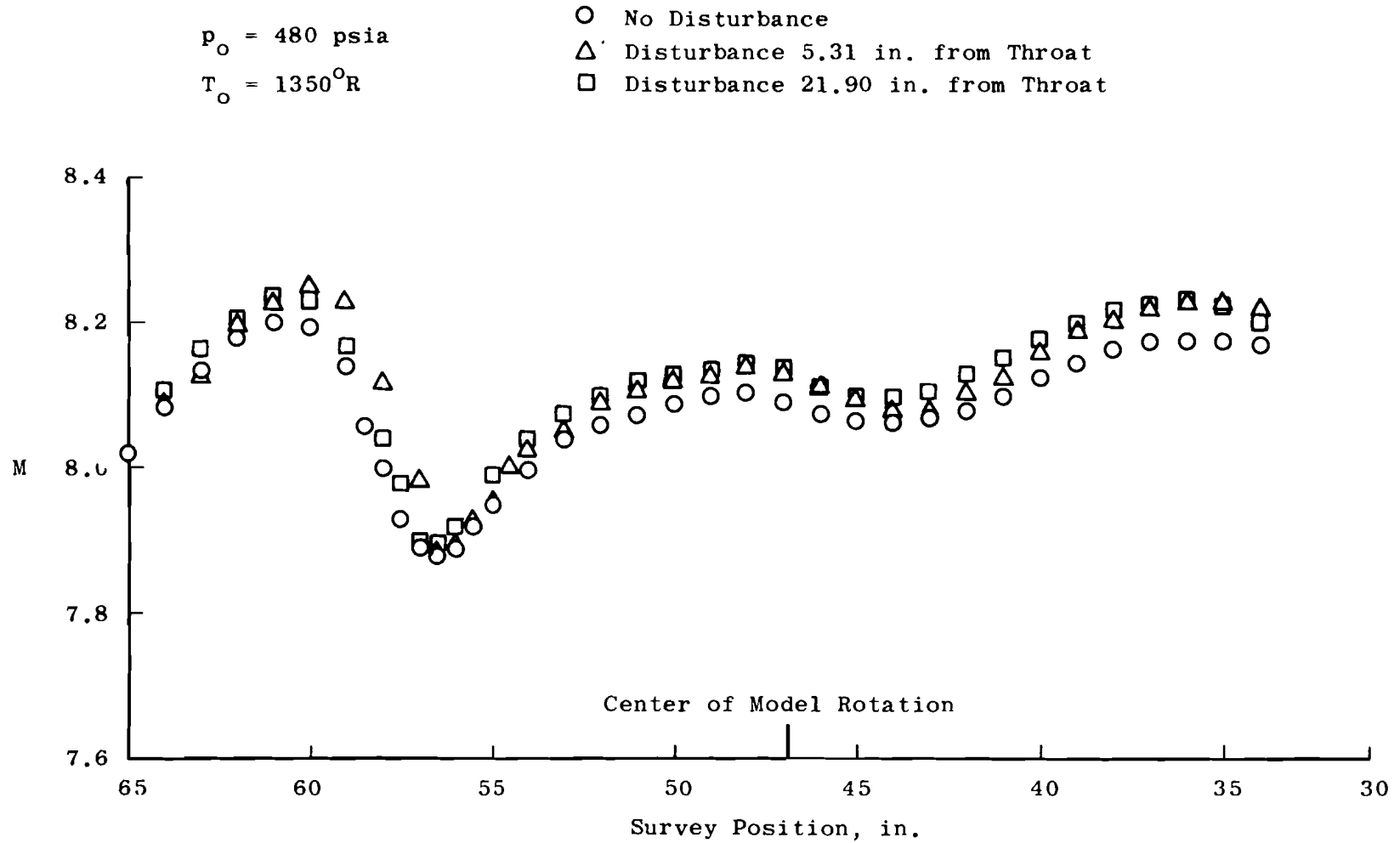


Fig. 11 Centerline Mach Number Variation with and without Known Disturbances

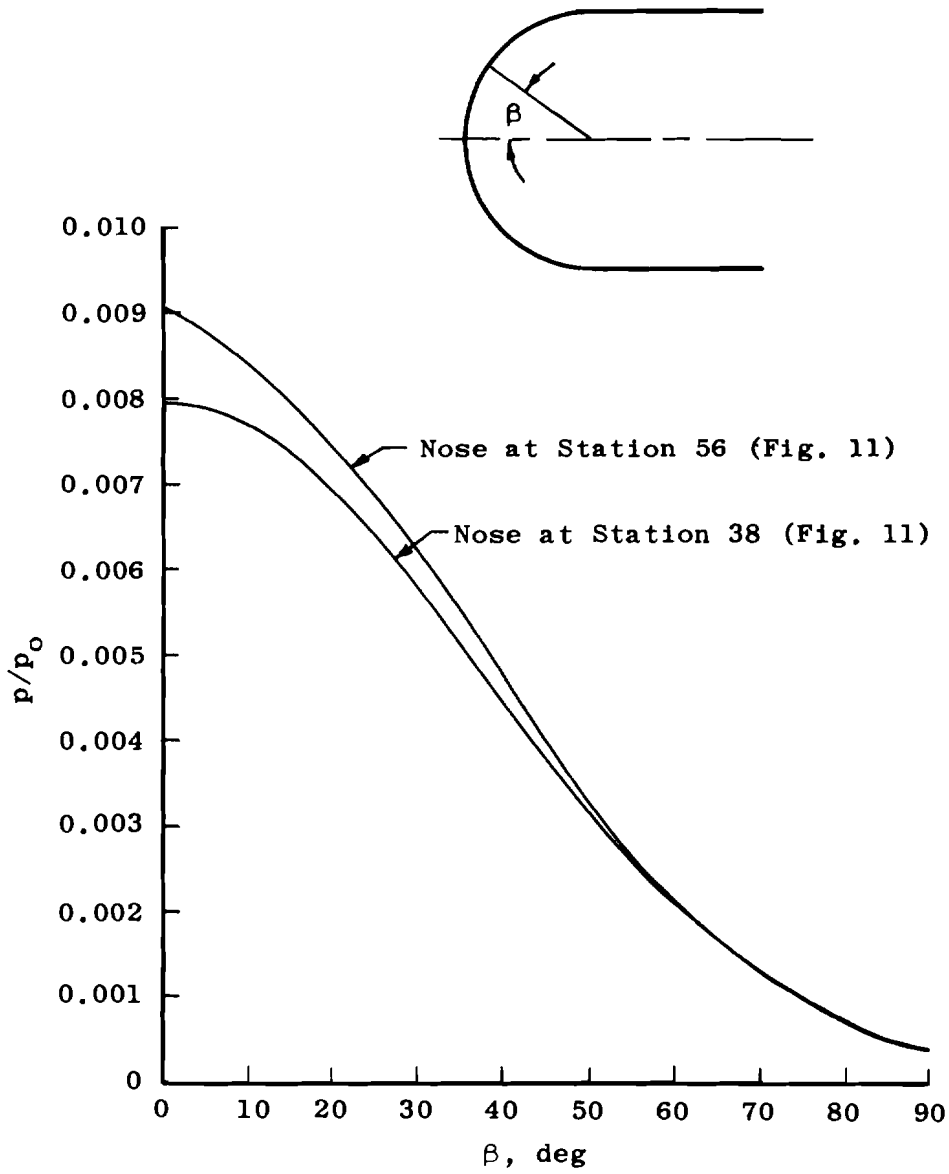


Fig. 12 Pressure Distributions Measured on a Hemispherical Nose of a Model Located at Two Positions in the Mach 8 Tunnel (B)

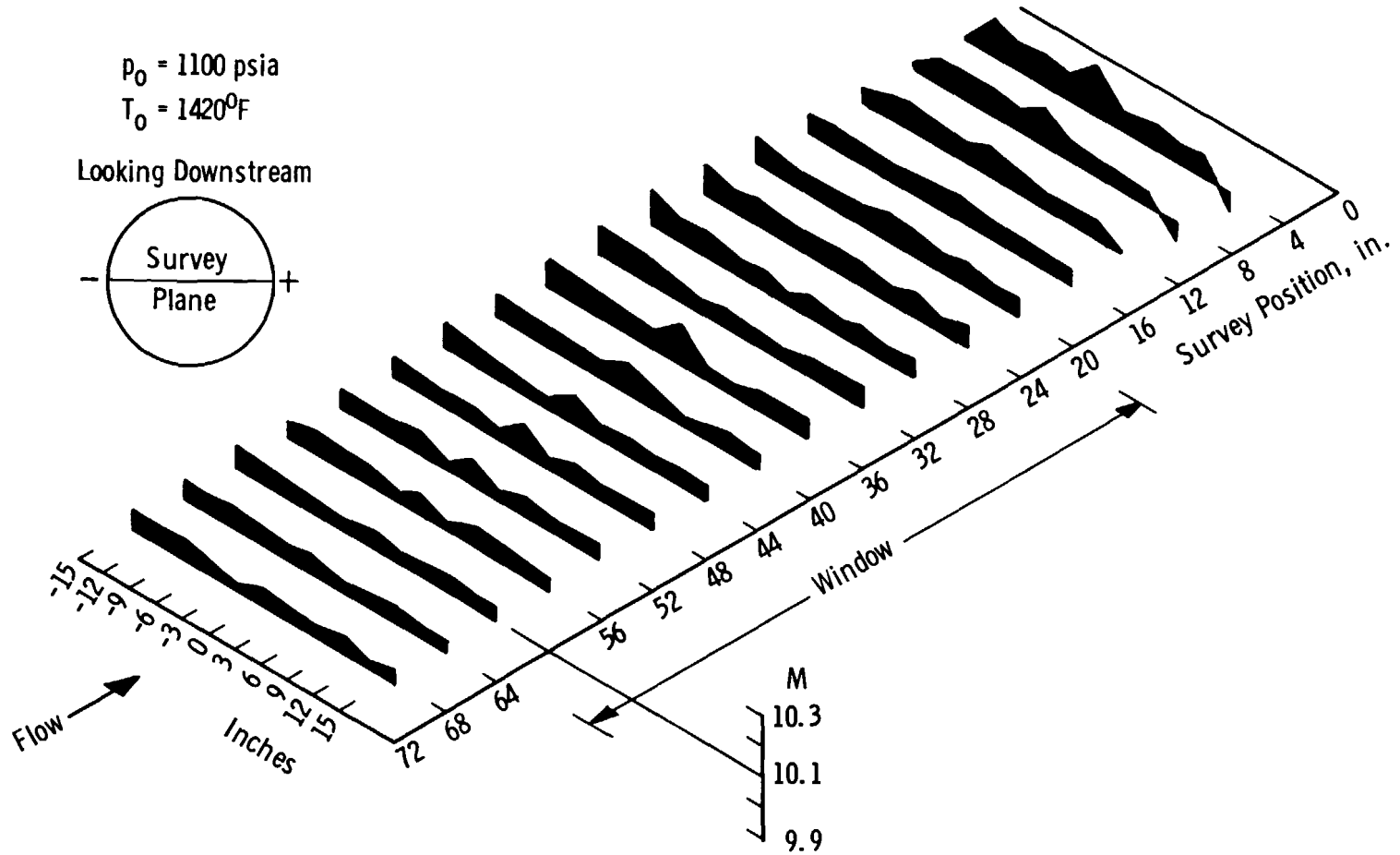


Fig. 13 Mach Number Distribution in the Mach 10 Tunnel (C)



Fig. 14 Shadowgram of Flow Angularity Probe